Title: Highly dispersed Fe^{3+}-Al_2O_3 for the Fenton-like oxidation of phenol in a continuous up-flow fixed bed reactor. Enhancing catalyst stability through operating conditions

Authors: Carla di Luca, Paola Massa, Javier M. Grau, Sergio G. Marchetti, Rosa Fenoglio, Patricia Haure

PII: S0926-3373(18)30456-9
DOI: https://doi.org/10.1016/j.apcatb.2018.05.032
Reference: APCATB 16686

To appear in: *Applied Catalysis B: Environmental*

Received date: 14-1-2018
Revised date: 6-5-2018
Accepted date: 10-5-2018

Please cite this article as: Luca Cd, Massa P, Grau JM, Marchetti SG, Fenoglio R, Haure P, Highly dispersed Fe^{3+}-Al_2O_3 for the Fenton-like oxidation of phenol in a continuous up-flow fixed bed reactor. Enhancing catalyst stability through operating conditions, *Applied Catalysis B: Environmental* (2018), https://doi.org/10.1016/j.apcatb.2018.05.032

Highly dispersed Fe^{3+}-Al_2O_3 for the Fenton-like oxidation of phenol in a continuous up-flow fixed bed reactor. Enhancing catalyst stability through operating conditions.

Carla di Luca[1,*], Paola Massa[1], Javier M. Grau[2], Sergio G. Marchetti[3], Rosa Fenoglio[1] and Patricia Haure[1]

[1] Departamento de Ingeniería Química-Facultad de Ingeniería, Universidad Nacional de Mar del Plata e Instituto de Ciencia y Tecnología de Materiales (INTEMA-CONICET), Av. J. B. Justo 4302 (B7608FDQ), Mar del Plata, Argentina.

[2] Instituto de Investigaciones en Catálisis y Petroquímica "Ing. José Miguel Parera"-INCAPE (FIQ, UNL-CONICET), CCT CONICET Santa Fe "Dr. Alberto Cassano", Colec. Ruta Nac. 168 Km 0, Paraje El Pozo (S3000AOJ), Santa Fe, Argentina.

[3] Departamento de Química- Facultad de Ciencias Exactas, Universidad Nacional de La Plata y Centro de Investigación y Desarrollo en Ciencias Aplicadas (CINDECA-CONICET), CICPBA, Calle 47 Nº 257 (B1900JK), La Plata, Argentina.

* Correspondence to: cardiluca@fi.mdp.edu.ar

Graphical abstract

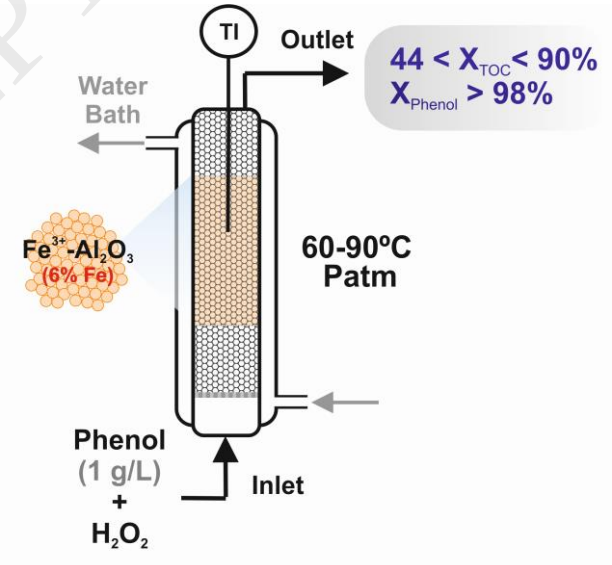

Highlights

- Enhanced synthetized Fe^{3+}-Al_2O_3 was tested for the continuous oxidation of phenol in an UFBR.
- 90% TOC reduction and leached Fe < 3 ppm were reached at selected operating conditions.
- Catalyst remained active after 70 h of usage with TOC reductions > 70%.
- Chelating by-products favored Fe lixiviation and Fe redistribution and poisoning by adsorption.
- Proper adjustment of operating conditions allowed minimize deactivation processes.

Abstract

A highly dispersed Fe^{3+}-Al_2O_3 catalyst (6 wt% Fe) was used for the catalytic wet hydrogen peroxide oxidation of phenol (1 g/L) in an up-flow fixed bed reactor (UFBR) under continuous operation. To enhance catalytic performance, three simple synthesis strategies were combined: two-stage impregnation of iron citrate, acid washing with CH_3COOH and thermal treatment at 900 ºC. Solid samples were characterized in depth by several techniques: N_2 Physisorption, XRD, SEM–EDS, TEM, TGA, PZC, TPD of pyridine, XPS and Mössbauer. Peroxidation experiments were performed in an UFBR over a wide range of operating parameters in order to evaluate their influence on phenol mineralization and catalyst stability. Under selected operating condition (T = 90 °C, W_{cat} = 20 g, Q_L = 1.2 mL/min and $[H_2O_2]$:[Phenol] = 16.8), complete phenol conversion and remarkable TOC reduction of 90% were achieved, with a high H_2O_2 consumption efficiency (η = 76 %) and low Fe leaching (< 3 mg/L). After 70 h of usage at different steady state conditions, the catalyst retained high mineralization levels (X_{TOC} > 70%) but the cumulative iron loss was calculated to be c.a. 20% of the initial Fe loaded in the UFBR. The catalyst was susceptible to leaching due to the accumulation of complexing intermediates such as carboxylic acids. However, acceptable iron leaching values (< 10 mg/L) were achieved when the reactor operating conditions were properly set (55% < X_{TOC} > 80%). The presence of chelating by-products favored also the Fe redistribution inside the catalyst pellets. Nevertheless, catalyst decay in the long-term operation was mainly due to the occurrence and permanence of chelating organic acids. This process

was specially promoted by the amphoteric character of the alumina-based catalyst. However, adsorbed species were promptly eliminated by calcination at 500 ºC, recovering steady state conversion profiles.

Keywords: Fe3+-Al2O3; phenol removal; continuous fixed bed reactor;chelating intermediates; catalyst deactivation.

Nomenclature

D_i: internal diameter of the reactor (cm)

D_p: diameter of catalyst particle (mm)

UFBR: up-flow fixed bed reactor

k_{ap}: apparent rate constant (min^{-1})

L: height of the column (cm)

Q_L: total flow rate (mL/min)

TOS: time on stream (h)

V_L: liquid volume (mL)

V_b: bed volume (mL)

W_{cat}: catalyst load (g)

Z: height of the bed (cm)

ε: bed porosity

ε_L: liquid hold-up

η: efficiency of hydrogen peroxide consumption (%)

θ: residence time (min)

1. Introduction

Nowadays, the world is facing a water crisis related to an exponential growing population, larger industrial requirements and the discharge of untreated and/or partially-treated wastewaters. As future projections reveal that by 2050, water demand will increase by 55% [1], it is essential to advance in the development of more efficient wastewater treatment technologies.

Over the last few decades, Advanced Oxidation Processes (AOPs) have shown encouraging performance over conventional water treatment technologies [2]. Generally, AOPs are based on the *in-situ* generation of a powerful oxidizing agent, such as hydroxyl radicals (•OH), to achieve the complete abatement and high mineralization

levels of toxic and refractory organic pollutants at moderate operating conditions. Main types of AOPs are based on the production of hydroxyl radicals through chemical, photochemical, sonochemical and electrochemical reactions [3]. Among them, the so-called heterogeneous Fenton systems combine the advantages of classic Fenton oxidation: inexpensive chemicals, moderate operating conditions, simple implementation in existing plants, etc.; with the ones from heterogeneous catalysis: easy separation and reusability of the catalyst without formation of Fe sludge.

Typically, heterogeneous Fenton catalysts are based on the immobilization of transition metals (mainly Fe) onto different porous matrixes such as activated carbon [4], silica [5], alumina [6–8], pillared clays or zeolites [9,10], among others [11]. In particular, Fe/γ-Al_2O_3 based catalysts may display enhanced catalytic performance due to the amphoteric nature and good adsorption characteristics of the alumina support combined with the development of advantageous Fe-Al interactions [12–14]. During the impregnation process of these catalysts, the characteristic Lewis acidity of alumina promotes high dispersion of Fe species, increasing the number of available active sites. In addition, alumina Lewis acidity might facilitate the redox cycle of Fenton mechanism [14]. On the other hand, the alumina adsorption ability towards organic and inorganic molecules may contribute to catalyst deactivation if the adsorbed molecules do not further react under reaction conditions. Adsorption of organic compounds might be influenced by surface characteristics (surface area, pore volume, pore size distribution, pH_{PZC}), pH and composition of the aqueous effluent [15]. Therefore, the function of Al on the high reactivity towards Fenton reaction needs further research [13].

Besides the good perspective of heterogeneously catalyzed Fenton system at batch scale, further engineering research must be performed in continuous systems (fixed-bed, fluidized-bed and continuous stirred-tank reactors) in order to allow large-scale applications [2,11,16].

Over the last two decades, heterogeneous Fenton/Fenton-like processes were extensively studied by using discontinuous batch reactors, which often are not the best solution for continuously generated industrial effluents. In recent years, more attention has been given towards their use in continuous treatment systems. Estevez et al. recently reviewed the literature devoted to the application of continuous reactors (fixed-bed, fluidized-bed and continuous stirred-tank reactors) for the treatment of model compounds and industrial wastewaters. The authors give examples of the most up-to-date findings in the research field, the advantages and disadvantages of each reactor

configuration, along with a complete revision of the most relevant operating parameters [16].

In particular, fixed bed reactors (FBR) are attractive configurations that allow amplifying the solid to liquid ratio, which accelerates the mineralization of the organic pollutant and increases the treated volume of effluent by using shorter contact times. The liquid flow is usually directed upwards to prevent formation of gas pockets, to enable gas bubbles to leave through the top and to ensure that the catalyst is completely wetted. The main advantages over stirred-tank reactors or slurry bubble columns with suspended catalysts are the well specified residence time with minimum backmixing and the fixed catalyst bed, which avoids separation of the solid catalyst [17]. This configuration also avoids mechanical degradation by attrition/crushing of the catalyst due to agitation. Continuous FBR have been used in heterogeneous Fenton-like processes applied to the treatment of pharmaceutical [18] and textile [4] wastewaters, in dye removal [4,19] and oxidation of phenolic solutions [5,10,20–22].

Catalyst deactivation is undoubtedly a concern in the practice of industrial processes. In fact, heterogeneous Fenton-type oxidation was associated with different deactivation mechanisms: i) leaching of active species, ii) fouling by accumulation of carbonaceous deposits, iii) poisoning by adsorption of complexing organic intermediaries and iv) attrition by reduction of the catalyst specific surface area [11]. It is widely accepted that leaching of active species is mainly associated with the accumulation of carboxylic acids of chelating nature such as oxalic acid [7,23] more than with the acidic pH of reaction medium [24]; the concentration of chelating organic acids strongly depends on operating conditions and the solid catalyst features [23]. On the other hand, fouling of catalyst surface by formation of carbonaceous deposits has been widely reported in studies of Catalytic Wet Air Oxidation (CWAO) [25,26]. Though, some publications of heterogeneous Fenton-type oxidation have reported noticeable surface modifications, by the accumulation of polymeric deposits that were eliminated after thermal treatment at 450 ºC [27,28]. Another mechanism scarcely reported is the strong adsorption of several of the reactants or reaction products (in particular, organic acids) that can block surface reactivity by poisoning and also modify the surface charge of the material altering the diffusion rate of anions, radicals and organic molecules [23,29].

The removal of phenols and their derivatives constitutes a research field of vast activity due to its elevated occurrence in various industrial wastewaters [30]. Hence, phenol was chosen as a model pollutant due to its elevated toxicity and refractory nature (poor

biodegradability) by means of conventional treatment technologies. A high initial concentration was set (1 g/L) in order to test the solid catalyst under more demanding conditions.

In this contribution, we present a deep characterization of the Fe^{3+}-Al_2O_3 catalyst and its performance for the phenol peroxidation carried out in a continuous UFBR. Our research aims to: (1) implement simple and cheap preparation strategies to improve the catalytic performance of heterogeneous Fenton-like systems that result active, stable and economic; (2) give a comprehensive description of the studied material and understand its surface and structural properties connected with its catalytic behavior; (3) provide detailed information on the start-up and performance of a continuous UFBR; (4) assess the catalytic performance under a wide range of operating conditions; (5) give some light over the role of electrostatic interactions between the organic molecules and the amphoteric iron-alumina catalyst (6) appraise the nature of deactivation processes in the long-term operation and (7) select proper operating conditions in order to minimize catalyst deactivation.

2. Experimental section

2.1. Preparation of Fe^{3+}-Al_2O_3 catalyst

The Fe^{3+}-Al_2O_3 catalyst (6 wt% Fe) was prepared by incipient wetness impregnation of iron citrate (Aldrich, technical grade) onto commercial alumina spheres (SASOL, Dp = 2.5 mm) at the best conditions described elsewhere [31]. Typically, heterogeneous Fenton-like catalysts based on iron employ ferric nitrate as metal precursor salt [7,8]. However, the Fe-catalysts prepared using this precursor showed poor dispersion levels; whereas the use of chelating precursors (as citrate) promoted homogeneous distributions of Fe due to a change of viscosity of the impregnating solution during the drying step. As a result, the formation of oxide clusters is avoided (silent iron phases on XRD) while a uniform distribution of the active component over the support bodies is favored [31,32]. The impregnation procedure was carried out in two consecutive stages by adding half of the total iron load at each step. After each impregnation, the sample was left for 12 h at room temperature and dried for 24 h at 150 °C. Dried samples were calcined at 900 °C in a muffle furnace with integrated air circulation for 4 h (10 °C/min). With the aim of removing less stabilized Fe species, the calcined material was acid-washed into an aqueous solution of acetic acid (1 mol/L) for 24 h at room

temperature. This short-chain organic acid was selected since it is widely recognized as a refractory by-product of phenol oxidation [33,34]. Afterwards, the catalyst was thoroughly rinsed with distilled water, dried at 150 °C and re-calcined at 900 °C for 2 h. The catalyst was labeled as Fe900ac.

2.2. Catalyst characterization

Characteristics of the alumina support and Fe^{3+}-Al_2O_3 catalyst were determined by different conventional techniques.

The nitrogen adsorption and desorption isotherms at -196 °C were measured using a Quadrasorb SI equipment. Specific surface areas of the mesoporous catalysts were calculated from the adsorption branches by the BET method, while pore volumes and pore diameter sizes were obtained by the NLDFT equilibrium method in the relative pressure range of 0.00 – 1.00 (c.a. 40 – 760 mmHg) [35]. Before analysis, each sample was degassed overnight at 120 °C under vacuum conditions.

Powder X-Ray Diffraction (XRD) of the catalyst samples were obtained with a PANalytical X'Pert Pro diffractometer by using CuKα radiation (λ = 1.54056 Å). The diffractograms were recorded over $10° < 2\theta < 70°$ range and compared to the JCPDS files to confirm phase identities.

The catalyst surface was investigated by Scanning Electron Microscopy (SEM) using a JEOL JSM-6460LV electronic microscope. The elemental composition was determined by energy dispersive X-Ray spectroscopy (EDAX) using an EDAX Genesis XM4-Sys60 equipment. Samples were metallized with Au or Au-Pd in a sputtering device Denton Vacuum Desk II**.**

The microstructure of the materials was studied by Transmission Electron Microscopy (TEM) using a JEOL TEM-1011 instrument. Samples were prepared by dispersing the powdered catalysts in ethanol and dropping the suspension onto a standard formvar-coated copper grid.

X-Ray Photoelectron Spectroscopy (XPS) was employed for surface iron analysis using a multi-technique system (SPECS) equipped with a conventional dual Mg/Al X-ray source and a Phoibos 150 analyzer operating in the fixed analyzer transmission (FAT) mode. Spectra were recorded at a pressure below 2×10^{-8} mbar. Binding energies were referred to adventitious carbon at 285 eV. The data treatment was performed with the Casa XPS Processing Software.

The Mössbauer spectra were obtained in transmission geometry with a 512-channel constant acceleration spectrometer. A source of 57Co in Rh matrix of nominally 50 mCi was used. Velocity calibration was performed against a 12-μm-thick α-Fe foil. All isomer shifts (δ) mentioned in this paper are referred to this standard at room temperature. Temperature was varied between 13 and 298 K working with an ARS closed-cycle cryogenic system. The Mössbauer spectra were evaluated using a commercial program with constraints named Recoil [36]. The spectra were folded to minimize geometric effects.

The organic matter removal of the used catalysts was determined by Thermogravimetric Analysis (TGA) performed with a TGA Q500 V 20.13 (TA instruments) thermobalance under air atmosphere at a heating rate of 10 °C/min and a temperature interval between 50−800 °C.

The point of zero charge (PZC) and the surface charge were determined by the mass titration method following the protocol reported by Preočanin and Kallay [37]. Different catalyst masses were added to aqueous solutions of different initial pH values adjusted by addition of HNO_3 or KOH. During the experiment, the pH of each solution changes gradually and once equilibrated approaches a constant value, which is the PZC. The ionic strength was kept constant at 0.003 mol/L and controlled by KNO_3 as background electrolyte. The experiments were performed in a closed reactor of 50 mL at room temperature and the electrolyte was purged with nitrogen in order to avoid the influence of atmospheric carbon dioxide. The pH value of the solution was measured after equilibration by using a Black Stone pH controller.

The quantity and amount of acid sites was assessed by means of temperature programmed desorption of pyridine. 0.2 g of the catalyst was first immersed in a closed vial containing pure pyridine (Merck, 99.9%) for 4 h. Then the catalyst was taken out from the vial and excess pyridine was removed by evaporation at room temperature under a fume hood. The sample was then charged to a quartz microreactor and a constant nitrogen flow (40 mL/min) was established. Weakly adsorbed pyridine was first desorbed in a first stage of stabilization by heating the sample at 100 °C for 2 h. The temperature of the oven was then raised to 700 °C at a heating rate of 10 °C/min. The reactor outlet was directly connected to a flame ionization detector to measure the desorption rate of pyridine.

Total Fe concentration was determined by a standard colorimetric test (FerroVer®Iron Reagent, HACH). The iron content of fresh catalyst was measured over solid samples

previously digested in HNO_3−HF. In order to ensure the reproducibility of the determined concentrations, the reported values are the average of at least two different samples, each one measured in duplicate during the standard colorimetric method.

2.3. Catalytic tests in an up-flow fixed bed reactor

The catalytic wet hydrogen peroxide oxidation (CWHPO) of phenol (1 g/L) was performed using the experimental set-up shown in Figure 1. The reactor consists in a glass jacketed column and the reaction temperature was kept constant by the upstream circulation of hot water throughout the reactor jacket. The column was divided in three distinguished zones: 1) pre-bed consisting of inert beads of the same size than the catalyst; 2) catalyst bed and 3) post-bed of inert beads. Experiments with smaller catalyst loads (W_{cat}) required a higher load of inert glass spheres to assure constant length of the column. The length of the pre-bed was increased accordingly, but the height of post-bed remained constant throughout the different experiments to preserve the response time of the system. The feed solution was pre-heated in a thermostatic bath and pumped to the column in up-flow mode by means of a peristaltic pump. This scheme ensures complete catalyst wetting. The oxidant dosage was adjusted to different molar ratios in order to maintain the mineralization levels as high as possible. Reactor features and operating conditions are listed in Table 1.

The liquid residence time (θ) was calculated following the procedure reported by Martínez et al. [5,38]. This method takes into account the physical properties of the fluids (liquid and gas), operating conditions and geometrical properties of the UFBR. For CWHPO tests, the gas phase is formed by carbon dioxide from organics mineralization and oxygen from parasitic decomposition of H_2O_2. Bearing in mind this, a conservative estimation of gas phase velocity allowed to approximate the liquid hold-up (ε_L) as the bed porosity (ε), assumed as the theorical value for loose random packing of spheres ε = 0.4 [39]. Thus, the residence time depends on the simultaneous adjustment of the total flow rate (Q_L) and W_{cat}. For the operating conditions used in this work, θ was varied between 1.1 – 15 min and was considered as defined in Eq. (1):

$$\theta = \frac{V_l}{Q_L} = \varepsilon \cdot \frac{V_b}{Q_L} \qquad (1)$$

Where the bed volume (V_b) was calculated from the height of the bed (Z) and the cross section of the column.

The percentage efficiency of hydrogen peroxide consumption η was calculated according to Eq. (2). The ratio R corresponds to the ratio between the experimental oxidant to phenol molar ratio and 14 (theoretical stoichiometric ratio for complete phenol oxidation). This definition contemplates that by feeding a suprastoichiometric oxidant dosage, η values cannot reach 100%.

$$\eta\ (\%) = \frac{gTOC_{converted}/gTOC_{initial}}{gH2O2_{converted}/gH2O2_{initial}} \cdot \frac{100}{R} \qquad (2)$$

In addition, preliminary and complementary batch tests were performed by using an experimental set-up as described elsewhere [12].

2.4. Analytical techniques

During experiments, liquid samples were regularly taken at the column top and immediately analyzed in order to evaluate phenol and total organic carbon (TOC) removal, hydrogen peroxide consumption, pH evolution, UV absorption of aromatics at 254 nm and Fe leaching.

Phenol and hydrogen peroxide concentrations were determined by standard analytical techniques, colorimetric method and iodometric titration respectively [40]. TOC contents were measured at least in duplicate by using a Shimadzu TOC-VCPN analyzer. The removal of aromaticity was measured at 254 nm (diluted 1:16) with a Shimadzu UV-1800 spectrophotometer and reported as dimensionless ratios in relation with a fresh phenol solution (UV_{254}). The pH was determined by using a Black Stone pH controller.

The Fe leaching levels in the outlet of the reactor were determined over liquid samples from the collected effluent by a standard colorimetric test (FerroVer®Iron Reagent, HACH). The cumulative loss of iron as a fraction of the initial Fe content was calculated according to Eq. (3):

$$Fe_{leached} = \int_0^t C_{Fe} \cdot Q_L \cdot dt \qquad (3)$$

By taking into account the feed flow rate (Q_L), the output concentration of Fe (C_{Fe}) and the time on stream (TOS) under continuous operation at each steady state for W_{cat} = 20 g [4].

In order to confirm the repeatability of experiments, steady-state outcomes of a representative reaction condition (80 °C, Q_L = 5 mL/min) was periodically verified.

3. Results and discussion

3.1. Characterization results

Surface and structural characteristics of metal oxide catalysts strongly affect physicochemical properties and catalytic behavior (activity, selectivity, stability, etc.). Hence, alumina support and fresh catalyst samples were thoroughly characterized by different techniques.

Physisorption of nitrogen revealed that the treated catalyst retained main surface characteristics of the mesoporous alumina support. However, it should to be note that calcination stage at 900 ºC diminished the surface area of the commercial alumina support in a 34% and provoked a noticeable change of the mean pore diameter (Table 2). All adsorption/desorption isotherms were type IV with H1–H3 hysteresis loops indicating capillary condensation taking place in mesopores (Figure 2-a) [35]. The materials exhibited a narrow pore size distribution between 30 – 50 Å (Figure 2-b) and a pore volume of ~ 0.4 cm^3/g typical for commercial γ-Al_2O_3 [41]. As seen in Table 2 both the impregnation process carried out in one-stage (Fe900-1s) and the thermal treatment at 900 °C (Al_2O_3-900) induced a reduction in surface area and pore volume due to partial pore blockage and surface shrinking respectively; whereas the two-stage impregnated catalyst (Fe900-2s) retained the area of the calcined support (Al_2O_3-900) prompting a better Fe distribution. The acid treatment (Fe900ac) reduced c.a. 10% of the Fe content in Fe900-2e, inducing an area reduction but recovering the pore diameter of the calcined support (Al_2O_3-900). The pore size distribution might suggest that acid wash removed the more labile Fe atoms that did not form part of the support structure and were blocking its porosity. The Fe species not eliminated during washing could be considered as better anchored to the alumina matrix conducing to more stable Fenton-like catalysts.

XRD results confirmed the high dispersion level of Fe species onto the alumina support displaying only γ-Al_2O_3 characteristic peaks (Figure 3). For samples calcined at 900 °C the diffraction rays get sharper and evolve towards rays which can be assigned to δ-

and/or θ-phases, in agreement with similar findings on boehmite-derived γ-Al_2O_3 reported by other authors [42,43]. Iron oxide phases were not detected neither the presence of mixed oxides due to the good dispersion of the active phase and the low total Fe content [44]. In order to obtain evidences about the Fe state, the diffractogram of the catalyst calcined at 1400 °C was performed (Fe1400). Even at this high calcination temperature, the existence of iron phases was not registered. Therefore, as a first approximation, the presence of FeO_x clusters in Fe/Al_2O_3 could be discarded, because is unlikely that this high calcination temperature does not produce sintering. If this process would occur, nanoparticles of α-Fe_2O_3 would be obtained (this is the iron oxide species more thermodynamically stable [45]. In a system of α-Al_2O_3, with α-Fe_2O_3 nanoparticles and 6 % wt/wt of iron loading, at least weak signals of this oxide would be detected by XRD. However, only the presence of α-Al_2O_3 peaks are recognized with their position slightly displaced in 2θ. Bearing in mind that Fe^{3+} and Al^{3+} ions have identical nominal charge and close ionic radii (r_{Fe3+} = 0.64 Å vs. r_{Al3+} = 0.51 Å) an isomorphic substitution of Al^{3+} by Fe^{3+} ions is possible [46]. This substitution would produce a small structural alumina matrix distortion, bringing about the displacement of the XRD peaks.

In agreement with XRD results, SEM-EDAX mapping and FeK-line profile exposed a uniform Fe distribution onto the alumina support and throughout the pellet cut (Figure 4). SEM micrograph shown in Figure 4-a is representative of the surface topography of the support and the iron-alumina catalyst. Likewise, SEM micrographs for commercial alumina, Al2O3-900, Fe900(2s), Fe900ac and used catalyst sample resulted analogous displaying no surface topography differences; unlike Fe900(1s), where some iron oxide clusters might accumulate on the catalyst surface after the impregnation step (see Figure S1 in the Supplementary Section). EDAX results showed that the metal is homogeneously dispersed onto the support and its weight percentage of 6.2 wt% (measured through different regions of the pellets) can be well compared with the Fe content of the bulk catalyst. However, the pellet outer shell has a slightly higher average weight percentage of 7.8 wt% Fe.

As can be observed from TEM image (Figure 4-b), the catalyst microstructure is constituted by compact and disordered grouping of plate-like primary particles, typical of mixed oxides systems. The stacking of these particles results in a tridimensional structure with narrow channels that constitutes the porosity of the material (as was detected by N_2 physisorption).

Figure 6 shows the XPS spectrum of Fe 2p. As can be seen, the Fe900ac sample shows binding energies at 711.4 and 725.0 eV for the photoelectron peaks of Fe $2p_{3/2}$ and $2p_{1/2}$, respectively. Various iron oxides and/or oxy-hydroxides have a similar range of Fe 2p binding energies [47]. Taking into account the previous thermal treatment of this solid (calcination in air at 900°C during a total time of 6 h) the only iron compound that could be present would be α-Fe_2O_3. However, the characteristic satellite peak of this compound, at about 719.0 eV, is not present. Consequently the presence of α-Fe_2O_3 must be discarded [48,49] Therefore, the peaks at 711.4 and 725.0 eV could be assigned to Fe^{3+} ions isolated with a surrounding of $O^{=}$ ions.

On the other hand, the chemical environment and oxidation state of Fe in the sample were investigated by Mössbauer spectroscopy. The Mössbauer spectrum of Fe900ac at 298 K only shows two peaks in the central region (Figure 7). This spectrum was fitted with a doublet and their hyperfine parameters (Table 3) could be assigned to paramagnetic Fe^{3+} ions and/or superparamagnetic iron species (with very small size), such as α-Fe_2O_3, γ-Fe_2O_3 [50,51], $FeAlO_3$ [52], etc. The presence of hercynite ($FeAl_2O_4$) can be discarded because it was not detected any iron species with isomer shift characteristic of Fe^{2+} [53].

With the aim to discern between the different possible iron species, the Mössbauer spectrum at 13 K was obtained (Figure 7). Again, only two central peaks were detected and the spectrum was fitted with one doublet. If superparamagnetic species would be present, when the measurement temperature decreases, a magnetic blocking occurs and the doublet is transformed into a sextuplet. It could be considered that a temperature lower than 13 K is necessary to produce this effect. However, α-Fe_2O_3 nanoparticles as small as 6 nm of size are close to complete its magnetic blocking at 30 K and the central doublet practically has disappeared to generate a sextuplet [54]. If α-Fe_2O_3 nanoparticles would be present is unlikely that, after the thermal treatment, they have sizes lower than 6 nm. Thereby, a sextuplet would be detected. Besides, the magnetic blocking is not a first order transition. Therefore, there is a broad temperature range in which the superparamagnetic relaxation is gradually slowed down. Consequently, the background of the spectrum shows a pronounced curvature. None of these phenomena is detected. Thereby, the presence of superparamagnetic nanoparticles of iron oxides can be discarded. On the other hand, $FeAlO_3$ at low temperature shows four sextuplets [55]. As a consequence, the existence of this species can be ruled out, too.

From the cross-checking of the XRD, XPS and Mössbauer results, we can conclude that paramagnetic Fe^{3+} ions are present in Fe900ac. They arise from the substitution of aluminum by iron ions; as was stated before, the isomorphic substitution is possible due to the identical nominal charge and similar ionic radii of Fe^{3+} and Al^{3+} ions. In the present system we have a transition alumina as support, either γ-alumina, or, more likely, θ-alumina (see diffuse X-Ray peaks in Figure 3) indicating that there are two types of aluminum sites: octahedral and tetrahedral. Bearing in mind that only one doublet was necessary to fit the Mössbauer spectrum at 13 K and considering that the isomer shift of Fe^{3+} ions located into tetrahedral sites is lower than that located in octahedral sites we can conclude that, in our system, paramagnetic iron ions are located in octahedral sites [56].

The quadrupole splitting value depends on the magnitude of the electric field gradient at the ^{57}Fe nucleus due to the local crystalline structure. The high values obtained for this hyperfine parameter, at both temperatures, would indicate that these paramagnetic Fe^{3+} ions are inside of highly distorted octahedral sites. Probably, they are on the alumina surface.

Therefore, from XPS spectra, XRD diffractograms, and Mössbauer spectra measured at 298 and 13 K we can conclude that all iron loading is present as paramagnetic Fe^{3+} ions located inside of distorted octahedral sites on the surface alumina. It can be speculated that Fe^{3+} ions diffuse inside the alumina lattice during thermal treatment at 900 °C.

Apart from catalyst structure characterizations and chemical environment of the doped Fe species, the assessment of surface reactivity results essential. So far, not much attention has been paid to the role of acid-base interactions in the use of heterogeneous Fenton catalysts. These concepts were first introduced in the study of catalytic ozonation processes and are thought to play a key role in the mechanisms of organic pollutants oxidation [57]. The interactions between active sites (highly dispersed iron centers included inside the alumina lattice), alumina host and the organic molecules might be an important point in the enhanced performance of the CWHPO of phenol by using iron-alumina systems [12,14,58]. These interactions strongly depend of the functional groups at the catalyst surface, the functional groups nature of the organic molecules (i.e. presence of carboxylic and phenolic-OH groups), the surface charge of the solid phase and consequently, of the effluent pH. The operation pH range will also affect the charge of ionic or ionisable organic molecules and also the charge of possible catalyst poisons. Therefore, the surface charge will influence the system sorption

behavior and consequently its catalytic performance [15,57]. Hence, determinations of the point zero charge and catalyst acidity are of crucial importance.

The point of zero charge (PZC) is a central concept in the adsorption of charged species and its position defines the affinity of the solid surface to the ionic species [59]. The PZC represents the pH at which the number of positively charges species ($M–OH_2^+$) equals the number of negatively charged species ($M–O^-$) nulling the net surface charge, where M stands for a surface metal center. In aqueous suspensions, ion exchange properties are based on the ability of surface hydroxyl groups (M–OH) to dissociate or to be protonated as a function of pH as follows [37,60]:

$$MOH + H^+ \rightarrow MOH_2^+$$
$$MOH + OH^- \rightarrow MO^- + H_2O$$

The PZC value was found to be c.a. 7.6 for the fresh commercial alumina and about 7.1 for the Fe900ac catalyst (Figure S2 in the Supplementary Section), which are consistent with those reported in the literature for similar metal oxide systems [59]. As is widely known, Fenton mechanisms greatly depend on pH and oxidations are typically carried out at acidic conditions. At the acid conditions used in this work (pH < 6) the catalyst surface should be positively charged and will adsorb/attract anions and/or negatively charged ligands from the aqueous effluent.

Catalytic properties of metal oxides are determined by its acidity and basicity. Hydroxyl groups are present on all metal oxides surfaces. These -OH groups formed at the surface behave as Brönsted acid sites, whereas Lewis acids and Lewis bases are sites located on metallic cations and coordinatively unsaturated oxygen, respectively. Both acid sites are thought to be the real catalytic centers of metal oxides [43,60]. For alumina based systems, the presence of active surface sites such as Lewis acid sites make them capable of behave as amphoteric ion exchangers depending on pH [59,60].

Figure 8 shows the evolution of pyridine desorption in nitrogen flow when the alumina and catalysts samples (Fe900(2s) and Fe900ac), saturated in pyridine and stabilized at 100 °C, are heated to 700 °C at 10 °C/min. In this evolution, the pyridine chemisorbed on centers of different acidic strength is desorbed as the temperature increases until completely desorbed. Thus, desorption curve quantifies the total amount of acid sites (weak, medium and strong acid sites) of each sample. The pyridine TPD results showed that the addition of Fe increased the acidity strength of the alumina support since all

desorption curves corresponding to catalysts with iron are displaced to higher temperatures and also higher concentration of acid sites (greater area under the curve). The acetic acid wash treatment (Fe900ac and Fe900(2s)), while eliminating 10% of Fe species weakly attached to the support, does not modify the acidity (total amount of acid sites and acidity strength).

From all these characterization results it can be established that the implemented strategies during preparation steps allowed the development of a highly dispersed Fe-alumina catalyst, with Fe species strongly anchored to the support. Higher Fe dispersion facilitates reduction-oxidation processes onto the solid catalyst surface [61] and also a faster H_2O_2 decomposition [62], by exhibiting a higher surface concentration of active sites and increasing the catalyst capability of producing radicals to carry out the oxidation of the organic molecules. On one hand, well-stabilized Fe species allows reducing the incidence of leaching processes associated with the acidic reaction medium and/or the accumulation of chelating carboxylic acids [31]. On the other hand, the amphoteric nature and the acidity of the iron-alumina catalyst might attract anionic intermediates towards the catalyst active centers, promoting its oxidation at proper operating conditions [15].

3.2. Peroxidation of phenol

3.2.1. Batch reactor experiments

The catalytic activity and stability of Fe^{3+}-Al_2O_3 material was tested for the hydrogen peroxide decomposition and for phenol peroxidation in a batch reactor.

The first approach to evaluate the catalyst performance was to test its ability to decompose H_2O_2 at different temperatures (in the absence of phenol) at $pH_0 = 5$ (which corresponds to double-distilled water matrix). A pseudo-first order kinetic model was used to fit the time evolution of H_2O_2 according with the mechanism proposed by Lin and Gurol [63]. From the pseudo-first order apparent rate constants enlisted in Table 4 (see Figure S3 in the Supplementary Section), the apparent activation energy was determined to be 38.5 kJ/mol ($R^2 = 0.9847$) in concordance with literature reports [63].

The peroxidation of phenol (1 g/L) at 70 °C was also tested in a batch reactor (Figure 9-a). Phenol was completely depleted in 120 min and high mineralization level (X_{TOC} = 80%) was observed after 240 min with a final Fe leaching of 2% (13 mg/L). As reaction time advanced, reaction medium color turned brownish and then transparent according

to the nature of reaction intermediates [33]. As seen in Figure 9-a, initial reaction rates of phenol, TOC and hydrogen peroxide (stage 1) are low and sharply increased to higher rates at c.a. 90 min (stage 2) as reaction evolved. To explain the differences in reaction rates observed, pH and Fe leaching values has to be taken into account. The pH decreased from the initial value (pH_0 = 6) to a minimum of 2.6 at 120 min and then slowly increases as time advanced. This clearly indicates the formation of acid intermediates that are further oxidized. On the other hand, the amount of leached Fe was negligible during the first 40 min and then increased. As reported before, Fe^{3+} heterogeneous systems applied to batch reactors exhibited a marked induction period for phenol and TOC abatement related with the activation of the catalyst surface under reaction conditions by means of two contributions: the presence of homogeneous Fe and the development of Fe^{2+}/ Fe^{3+} ratio [12,64]. Then, the lag phase observed in this experiment (stage 1) would be connected to the slow rate limiting reduction of Fe^{3+} by H_2O_2 and also with the build-up of Fe^{2+} species through faster pathways, such as the reduction of ferric species by quinone-like intermediates acting as electron-transfer catalysts [29,64].

Once the H_2O_2 was depleted at 120 min, an additional stoichiometric oxidant dose was supplied (stage 3) to further mineralize the organic matter. The TOC conversion increased up to a final value of 80 %.

Additionally, Figure 9-b shows the influence of phenol over the pseudo-first order apparent rate constants for hydrogen peroxide decomposition. During the first step (stage 1), the apparent constant rate (k_{ap} = 0.0049 min^{-1}, R^2 = 0.99) resulted 3.5 times smaller than the one reached in the absence of phenol due to competitive processes between phenol and the oxidant for the surface active sites. After 90 min (stage 2), the oxidant was decomposed about twenty times faster (k_{ap} = 0.1018 min^{-1}, R^2 = 0.99) than during the first stage, probably due to surface activation by the formation of ferrous species and/or the presence of homogeneous Fe species, which enhanced hydrogen peroxide decomposition. Afterwards, all H_2O_2 supplied was consumed and an additional stoichiometric dose was added to the reactor (stage 3), giving a constant rate comparable with the first stage (k_{ap} = 0.0067 min^{-1}, R^2 = 0.99).

Finally, the used catalyst was tested for peroxide decomposition in a blank without phenol (see Figure S3) achieving an apparent rate constant smaller than the one observed with the fresh catalyst and similar to the value evaluated in the presence of

phenol (k_{ap} = 0.0057 min^{-1}, R^2 = 0.99). This result indicates catalyst deactivation, whose origin will be discussed in detail in the next sections.

3.2.2. Up-flow fixed bed reactor under continuous operation

3.2.2.1. Blank experiments and start-up of the UFBR

According to the previous results, the iron-alumina catalyst was further investigated in a continuous UFBR. Contrasting with batch schemes, a very different catalytic performance can be expected in the fixed bed reactor due to its distinctive features: static solid phase, higher solid/liquid ratio, lower contact time between phases, etc. It is noteworthy to expect that the last two features may reduce leaching of Fe species.

Prior to core tests, several blank experiments were carried out in order to evaluate the potential contribution of non-catalytic mechanisms in phenol elimination and hydrogen peroxide decomposition. A blank test was carried out loading the column with 20 g of fresh alumina and negligible conversions of phenol, TOC and H_2O_2 in the outlet effluent were reached at typical operating conditions. In the absence of H_2O_2, phenol adsorption was negligible. As well, phenol, TOC and H_2O_2 concentrations were periodically verified in the feed tank to discard thermal depletion of reagents at the inlet supply, therefore ensuring initial concentrations.

Regarding to the start-up procedure with fresh catalyst loads, the following features were always observed. For instance, Figure 10 shows experimental results obtained at 70 °C, Q_L = 5 mL/min and pH_0=3 using fresh catalyst load. Before reaching steady state conversions, the conversion profiles displayed an induction period of about one hour. During the lag phase, as phenol and TOC conversion levels slowly increased, a brownish coloration of the solid phase was detected: a color front advanced slowly from the upper to the lower layers of the catalytic bed (Figure S4 at Supplementary Section). After the induction period, this coloration gradually disappeared and conversion levels reached steady state values: complete phenol abatement, 92 and 65% of H_2O_2 and TOC conversion, respectively and 36 mg/L of leached Fe. It should be noted that this phenomenon was even more pronounced when higher initial concentrations of phenol were used [65]. As discussed previously, the occurrence of color during early stages of phenol peroxidation is related to the presence of quinone-like intermediates. As reaction proceeds, these compounds are further oxidized and color disappears.

The oxidant profile showed a distinctive evolution. A minimum is observed at c.a. 60 min, starting from almost complete conversions due to parasitic decomposition (bubbles

are released at the top of the column). At 60 min, as catalyst is colored due to accumulation of quinone-like by-products on the catalyst surface, peroxide conversion decreased. Then, as the color front started to disappear, peroxide conversion increased up to the steady state value. As seen in Figure 10, during the lag phase the presence of leached Fe was negligible. Therefore, as in previous batch experiment, phenol oxidation began by a heterogeneous pathway that involves the surface accumulation of reducing organic intermediates that favors •OH production [64].

3.2.2.2. Influence of main operating parameters

The influence of main operating parameters, namely reactor temperature, residence time (by varying feed flow rate or W_{cat}), initial pH and adjustment of $[H_2O_2]$:[Phenol] ratio (R) on steady–state outcomes was explored. Results are summarized in Table 5.

As shown, phenol removal was above 98%, TOC conversions varied between 44-90%, aromaticity decreases as TOC conversions increases and η values exceeded 60%. Even though heterogeneous Fenton-like oxidation allows complete phenol removal and high mineralization levels, TOC conversion hardly reaches 100%. Therefore, the mass balance is completed considering the accumulation of by-products (see recognized intermediate species presented in Table S1 of the Supplementary Section). The first stage of the oxidation mechanism comprises phenol decomposition into aromatic compounds with two hydroxyl groups substituted in the benzene ring (hydroquinone, resorcinol and catechol). The oxidation of these molecules generates quinone-like compounds (p-benzoquinone and o-benzoquinone) which can be more toxic than phenol itself and adds color to the effluent. Besides, effluent coloration might be also due to the presence of quinhydrones and iron complexes. Then, oxidation of quinones gives place to the ring-opening of aromatic molecules to form carboxylic acids with lower carbon content which provoke the pH descent of the reaction medium [33,34]. Therefore, the organic carbon occurrence in the final effluent is related to the presence of strongly chelating and refractory carboxylic acids. These compounds favor the solubilization of the supported iron species. In general, these low chain organic acids are biodegradable and can be further degraded by means of subsequent biological treatment [66].

Results presented in Table 5 can be explained taking into account the oxidation mechanism. As observed, higher temperature (90 °C) intensified the oxidation process: hydrogen peroxide decomposition was accelerated and mineralization increased up to 90%. Therefore, removal of acidic intermediates was promoted and outlet pH values

increased. Consequently, Fe leaching decreased below 3 mg/L warranting better catalyst stability. In agreement, aromaticity of the treated effluent notably decreased.

The adjustment of initial pH did not enhance significantly the oxidation performance (see results at 70 °C, experiments SS5 and SS6). As discussed, the treatment of concentrated phenol solutions imposes a strong accumulation of acidic intermediates that contribute to work at pH values close to the optimal [67]. Therefore, CWHPO experiments were performed without initial pH adjustment (where pH_0 = 6 stands for the natural pH of a phenolic solution of 1 g/L), taking advantage of the natural decay of pH, without the needing of an additional acidification step.

From the result of pH_{PZC}= 7.1 obtained for the fresh Fe900ac catalyst, it could be inferred that acidic conditions may be more favorable to the efficiency of the oxidation process. Under these conditions, the positively charged catalyst surface could interact with anionic species from the aqueous medium (e.g. deprotonated reaction intermediates), promoting the adsorption of the organic compounds and their further oxidation. However, it should be noted that this PZC value expands the possibilities of using the catalyst within a wider range of pH, closer to neutrality. This might allow its application in the treatment of real wastewaters (with typically neutral pH values), minimizing additional steps of pH adjustments [16, 68]. In the following sections some other relevant aspects are also considered, as the incidence of different deactivation processes.

Hydrogen peroxide dosage was examined in order to get the maximum H_2O_2 consumption efficiency, maintaining the mineralization levels as high as possible. Excessive oxidant dosage should be avoided due to both the scavenging effect of hydroxyl radicals by H_2O_2 and the increase on the final cost of the process; however if hydrogen peroxide concentration is insufficient, the oxidation advance can be hindered. Hence, H_2O_2 fed was increased to a suprastoichiometric ratio of R = 16.8 in the experiments performed at temperatures above 70 °C. Particularly at this temperature (experiments SS5 and SS7), the increase of R resulted in an enhancement of 5% in TOC conversion. While η, aromaticity and final pH values remained constant and Fe leaching levels decreased more than 20%.

The impact of the residence time of the liquid phase θ on reactor performance was also addressed. In general, higher θ values increase mineralization and pH_{out}, hence the Fe leaching decreases.

As seen in Table 5, a relatively simple way to enhance catalytic performance might be to increase reactor temperature [69] and/or residence time. However, in terms of costs, it is always desirable to work at moderate temperatures and appropriate residence times, equilibrating operating conditions with the catalytic capability of the system under study. Moreover, the use of unreasonable high residence times will also increase the final cost of the process and its adequate adjustment must balance mineralization levels/Fe leaching in order to reduce the total treatment time and increase the treated effluent volume.

In summary, results presented in Table 5 evidence a relationship between TOC conversion values and Fe leached concentrations measured at the top of the column. Figure 11 shows this relationship under all tested operating conditions. A maxima concentration of leached iron at c.a. 60% of TOC reduction is observed. This is due to the presence of remnant organic matter with high concentration of chelating by-products that promotes iron dissolution. This relationship allows to establish an operating window in the range of $55 < X_{TOC} > 80\%$, in which the UFBR can be operated with Fe leaching levels below 10 mg/L.

Table 5 also compiles an estimation of the expected catalyst lifetime at each steady state. The lifecycles were estimated by considering the total Fe mass loaded to the UFBR, the feed flow rate and the steady state Fe leaching value. From these approximations, it can be observed that under optimized operating conditions the catalytic bed would work c.a. 300 h and beyond. Nevertheless, it should be noted that this approach only takes into account catalyst deactivation by Fe leaching and dismissed the incidence of other deactivation mechanisms which would influence the kinetic of deactivation, as will be discussed in the next sections.

3.2.2.3. Catalyst stability studies

Stability of the Fe-catalyst was evaluated at 80 °C and setting a residence time of θ = 3.7 min (experiment SS9 in Table 5). The catalyst was used 70 h, Figure 12 shows the profiles registered after 15 h of continuous mode operation at different steady state values. TOC and H_2O_2 conversion levels gradually decreased in c.a. 10% in the interval of time between 15–32 hours, retaining total phenol removal, outlet pH values around 2.7 and a constant Fe leaching of 15 mg/L (measured by the mixing cup method). The decline in TOC conversion caused an increase of the aromaticity and the treated solution becomes colored due to the presence of quinone-like by-products. It should be

remarked that these results compares reasonably well with the reference point SS9 listed in Table 5.

After 32 h of usage, different reactivation strategies were implemented in order to recover the initial steady state conversion levels and also to assess the nature of deactivation processes.

3.2.2.4. Catalyst deactivation

Catalyst deactivation in Fenton-like processes can be due to fouling by carbonaceous deposit, iron leaching and/or poisoning by adsorption of organic intermediates [11,23]. In addition, for the Fe-alumina catalyst used in this work, another source of catalyst deactivation was found. Additional experiments were performed to address these issues and results are presented in the next sections.

3.2.2.4.1. Carbonaceous deposits

TGA-DTA studies were performed over used catalyst samples in order to evaluate the removal of adsorbed organic intermediates and/or the presence of carbonaceous deposits (Figure S5 in the Supplementary Section). A loss weight of 2 wt% was registered in the range of 150-500 °C, with a pronounced step at 250 ºC. Since it is true that the analytical technique does not allow discerning about the nature of the removed organic matter, the surface of the used catalyst sample was analyzed by SEM trying to gather some evidence on the formation of carbonaceous deposits. Nevertheless, the micrograph displayed the same surface appearance that the fresh catalyst (See Figure S1 at the Supplementary Section).

Then, an additional experiment was performed with a sample of fresh catalyst exposed to a solution of oxalic acid at pH = 2.9 and succinctly analyzed by TGA-DTA (Figure S5 in the Supplementary Section). Again, the elimination of organic matter proceeded at 250°C, suggesting that the weight loss in the used catalyst sample corresponds to adsorbed carboxylic acids.

3.2.2.4.2. The question of Fe leaching

The Fe leaching by organic ligand promoted-dissolution of iron oxides was widely reported in the literature [29,70–72]. In summary, the dissolution of Fe-oxides takes place by different mechanisms such as protonation, complexation or reduction. The Fe dissolution by complexation is a surface-controlled reaction occurring in steps. First, the

fast adsorption of the ligand onto the oxide surface by a ligand exchange mechanism. Second, the surface complex slowly weakens the metal-oxygen bonds on the surface and finally detaches it from the crystalline lattice [29].

An important question regarding the heterogeneous Fenton systems performance is if the catalyst is truly heterogeneous or if the observed results are due to the presence of trace amounts of leached Fe.

Therefore, homogeneous Fenton tests with $Fe(SO_4).7H_2O$ at $pH_0 = 3$ were performed in a batch reactor at different temperatures and Fe^{2+} concentrations to characterize the influence of dissolved Fe at different operating conditions: 44 mg/L of Fe at 70ºC, 14 mg/L of Fe at 80ºC and 2 mg/L of Fe at 90ºC, equivalent to the measured Fe leaching in experiments SS5, SS9 and SS13 in Table 5. It should be noted, that these tests overestimated the homogeneous contribution since the release of Fe is a gradual process throughout the catalytic bed. For these experiments, no induction period was detected achieving TOC conversions of: 42% (44 mg/L of Fe at 70ºC), 39% (14 mg/L of Fe at 80 ºC) and 31% (2 mg/L of Fe at 90 ºC) after 10 min and TOC removals of: 61%, 58% and 51% after 120 min, respectively. Therefore, the influence of homogeneous iron as a secondary contribution of TOC mineralization might be strongly limited due to the short residence time at the UFBR and the good catalytic performance achieved could be mainly assigned to heterogeneous phenomena.

Moreover, it is broadly accepted that Fe leaching is mainly associated with the accumulation of oxalic acid. To assess its influence in the output effluent stream, we performed an additional heterogeneous batch experiment with oxalic acid at 80 ºC and 10 g/L of Fe900ac (setting a total carbon concentration of 191 mg/L, representing the 25% of remnant TOC for SS#9 in Table 5). This carboxylic acid confirmed its recalcitrant nature, reaching TOC conversions of 9% and 36% after 10 min and 120 min respectively. Iron was leached out of the catalyst during the first minutes of the reaction reaching values of 10 mg/L at 5 min, a maxima concentration of 19 mg/L at 30 min and a final value of 15 mg/L at 120 min. This experimental fact might indicate readsorption of leached Fe species, discarding iron precipitation at the acidic pH conditions of the reaction supernatant.

Noteworthy, homogeneous experiments were not performed under continuous operation in the UFBR because it is not possible to ensure identical residence times between heterogeneous and homogeneous tests. In our experimental setup, reaction will not only proceed in the inert glass bed. The reservoir, the enter and exit piping and the

unavoidable dead volumes in the inlet and outlet sections of the column will also contribute as additional contact time between the reactants. Therefore although batch tests are not representative of the continuous experiments, they serve as a good tool to evaluate the catalytic activity of the leached iron.

3.2.2.4.3. Intermediates adsorption

Heterogeneous Fenton-like oxidation is mainly driven by surface reaction mechanisms where different species compete for adsorption on the available surface active sites, leading to catalytic deactivation [13,29].

Interactions between organic ligands and metal oxide surfaces have attracted a great deal of attention due to their significant environmental implications. Adsorption of organic matter onto inorganic solid interfaces (e.g., Fe- and Al-phases) by means of surface complexation-ligand exchange mechanisms was widely reviewed in the literature of colloidal chemistry [73–78]. All these studies highlighted the fact that the degree of adsorption of organic compounds onto metal oxides surfaces is strongly dependent of: i) the pH value and ionic strength of the liquid phase, ii) the pH_{PZC} of the solid phase, iii) the number and nature of functional groups per organic molecule (i.e. -OH and -COOH), iv) the pKa of the dissociable groups and their steric arrangement. The adsorption of an organic molecule onto the alumina surface can be can be explained by the ligand-exchange model. Where the oxygen atom of the surface (-OH) group act as a donor (Lewis base) and coordinate with protons or metal ions (Lewis acids), whereas structural Al(III) ion present at the surface layer acts as a Lewis acid capable to exchange the (-OH) group for another anionic ligand [76].

Hidber et al. studied the adsorption behavior of different molecules based on a benzene ring substituted with (-OH) and (-COOH) groups and also aliphatic carboxylic acids onto α-Al_2O_3. The authors determined that the pKa value of the dissociable groups and the pH_{PZC} of the solid phase define the pH range at which the adsorption maximum occurs. Then, they stated that if the pKa < pH_{PZC} the adsorption maximum can be expected when pH ≈ pKa; but when pKa > pH_{PZC}, the adsorption maximum should occur around the pH_{PZC} of the material. Furthermore, the organic molecules with different functional groups can get a high degree of adsorption over a wide pH range between the pKa values of those dissociable groups. Consequently, whereas organic molecules with (-OH) groups (i.e. catechol) adsorbed preferentially in the high-pH regime, carboxylic acids showed strong adsorption in the low-pH region [76].

Therefore, taking into account the pKa values listed in Table S1 of the Supplementary Section and the acidic pH regime of the reactor (c.a. 6 – 2.6), it can be expected that the catalyst preferentially attracts carboxylic acids present as inner and outer-sphere complexes. Furthermore, the catalyst might develop greater adsorption affinity towards acids with more than one -COOH group, and especially those with cis-configured carboxylic groups (i.e. maleic acid) [77].

To confirm this deactivation hypothesis, the pH_{PZC} for the used catalyst was determined (over a solid sample taken out after c.a. 70 h of usage). As can be observed in Figure 13, the used catalyst displayed a shift of the pH_{PZC} by 2 pH units to lower values that reduces the positive surface charge in the range of pH = 4–6. According to the ligand-exchange model, the adsorption is a simple exchange of the -OH group for another dissociated group (i.e. -COOH) and does not necessarily lead to a change of the surface charge. However, the surface charge can be changed if the molecule has additional dissociated groups ('charge carriers') which are not coordinated to the surface or if two dissociated groups coordinate to the same Lewis acid center [73,76]. Following this reasoning, the pH_{PZC} decrease might be correlated with the permanent adsorption of anionic species such as dicarboxylic acids and/or more than one -COOH group coordinated to the same adsorption center. As a consequence of this shift, the role of electrostatic interactions at the solid–liquid interface would be changed, altering affinity between anionic ligands with the less positively charged catalyst surface.

Furthermore, TPD of pyridine were performed over the used catalyst sample (not shown). The spend catalyst showed to be much less acidic than the fresh sample. Nevertheless, the solid sample partially recovered its surface acidity after a thermal treatment at 500 ºC (2 h). This result is in agreement with the former hypothesis.

3.2.2.4.4. Iron redistribution

Iron leaching due to complexation was extensively discussed in the previous sections. However, complexing intermediates may also affect catalyst stability through another mechanism not previously discussed in the literature.

It was observed, after several hours of operation, the onset of color in the inner zone of the spherical pellets. According to Figure 14-a, the used catalyst presents an egg-yolk distribution that cannot be reverted by calcination at 500°C, discarding the accumulation of colored intermediates.

EDAX FeK profile displayed iron maxima in the inner region of the pellet and on its edge, reaching valleys between these regions and on the pellet center (Figure 14-b). Punctual determinations partially confirmed this trend (Figure 14-c), but absolutely contrast with the FeK profile of the fresh catalyst showed in Figure 5.

The Fe redistribution towards the core of the pellets might be favored by the presence of potential complexing agents; thus, iron-complexes could be considered as mobile species that gradually spreads over the alumina surface.

The phenomena can be compared with the competitive adsorption technique used in the preparation of egg-yolk type alumina catalysts [79,80]. These systems are based in the addition of a second component (polycarboxilic acid) that adsorbs more strongly than the metal precursor itself, leaving no available surface sites in the outer shell, causing the metal diffusion inward of catalyst grains in search for available sites [81].

Hence, besides Fe leaching detected in the liquid phase, complexed iron would be also re-dispersed inside of pellets. This non-homogeneous active site distribution adds an additional mass transport resistance (through the inner shell of support) that may contribute to the observed decrease in rates. On the other hand, Fe may not be well dispersed in the active inner core and this could also contribute to activity decay.

Considering the previous discussion, catalyst deactivation would be strongly related with the presence and permanence of chelating acidic intermediates. For alumina based catalysts, the amphoteric character of the support plays a key role by attracting anionic ligands towards Fe active centers. When operating conditions favor to shield high mineralization levels, the support aids to attract the organics intermediates towards Fe centers and mineralize them, leaving the active sites available for a new set of reactant molecules to attach to the catalyst surface. When more moderate reaction conditions are used, the system is not capable to mineralize the more refractory compounds such as acidic by-products and in consequence TOC conversions are low, the accumulated acidic intermediates remains more time adsorbed onto the surface and the catalyst is more prone to Fe dissolution [29]; hereafter, Fe species could be transferred to the liquid phase or be readsorbed/redistributed inside the spherical pellets.

3.2.2.5. Strategies for catalyst reactivation/regeneration

The effects caused by iron complexation (leaching and redistribution of iron inside the pellet) might be irreversible. However, adsorbed organic intermediates could be

removed to improve catalyst activity. Several reactivation strategies were tested in the UFBR and results on performance are shown in Figure 12.

First, reactor temperature was increased up to 90 °C (T1, Figure 12); however the system was not able to recover the steady state at 90 °C (SS11, Table 5) and the performance slightly descended to: X_{TOC} = 78%, X_{H2O2} = 87%, pH_{out} = 2.8, UV_{254} = 0.11, η_{H2O2} = 75% and $[Fe]_{leached}$ = 7.5 mg/L. When the reactor temperature was decreased again to 80 °C, conversion profiles recovered their previous descending tendency, reaching TOC conversions below 70% and $[Fe]_{leached}$ = 10.4 mg/L.

Second, the catalytic bed was dried at 150 °C for 72 h and then used in reaction (T2, Figure 12); again, the system recovered its descending profile of mineralization levels and an output concentration of dissolved Fe of 10.5 mg/L.

Afterwards, the catalyst was removed from the bed and calcined at 500 °C (2 h, static air atmosphere) to remove strongly adsorbed refractory by-products and then used again in reaction (T3, Figure 12). As observed, the catalyst exhibited the typical induction phase previously mentioned (Section 3.2.2.1) and during the steady state operation, the conversion profiles reestablished steady state values akin to those listed before (SS9, Table 5): X_{TOC} = 76%, X_{H2O2} = 88%, $[Fe]_{leached}$ = 11.8 mg/L, pH_{out} = 3 and η = 72%.

Finally, when mineralization levels decayed below X_{TOC} = 70%, a fourth reactivation strategy was tested (T4, Figure 12). This time the UFBR was softly washed with a 0.1 mol/L solution of NaOH (1 h at 80 °C) with the purpose of desorb adsorbed acidic intermediates [27]. The change of reaction medium pH did not allow recovering an average TOC conversion above 70% and the leached iron was 11 mg/L.

After 70 h of usage under continuous operation at different steady state conditions the cumulative loss of iron as a fraction of the initial Fe content loaded to the UFBR was calculated to be c.a. 20%.

4. Conclusions

A highly dispersed and well-anchored iron-alumina catalyst was synthetized and used for the CWHPO of concentrated phenolic solutions in a continuous UFBR. The preparation methodology involved the combination of three simple and cheap synthesis strategies (two-stage impregnation of iron citrate, acetic acid washing and thermal treatment at 900 ºC) that favored: i) high dispersion levels of Fe onto the mesoporous support, ii) the removal of the more labile Fe species and iii) the diffusion of Fe^{3+} inside the alumina lattice, giving rise to strong Fe-Al interactions.

Peroxidation of 1 g/L of phenol was performed over a wide range of demanding operating parameters. In all cases, phenol removal was above 98%, TOC conversions varied between 44-90% and H_2O_2 consumption efficiencies resulted $\eta > 60\%$. Under selected working condition (T = 90 °C, W_{cat} = 20 g, Q_L = 1.2 mL/min and $[H_2O_2]$:[Phenol] = 16.8), complete phenol conversion and remarkable TOC reduction of 90% were achieved, with less than 3 mg/L of iron leached. Although the catalyst was subject to deactivation, high mineralization levels (> 70%) were sustained for 70 h of continuous operation. Nevertheless, the UFBR usage at different steady state conditions with output Fe concentrations up to 44 mg/L caused a cumulative loss of iron c.a. 20%. The nature of deactivation processes in the long-term operation of the reactor was thoroughly characterized. Activity decay of the amphoteric Fe-Al catalysts is strongly related with the presence and permanence of chelating acidic intermediates. These chelating by-products diminished catalyst performance by different mechanisms:

a) Fe migration to the liquid phase as Fe leached species and to the catalyst pellets core giving egg-yolk distribution.

b) Permanent adsorption of carboxylic acids that block surface sites and modify affinity towards anionic ligands, affecting the conversion levels in the long-term operation. Nevertheless, adsorbed species were easily removed by calcination at 500 ºC, recovering steady state conversion profiles.

Therefore, the proper adjustment of operating conditions results decisive to prolong the useful life of the catalytic bed. Namely, the Fe leaching can be reduced to acceptable levels (< 10 mg/L) if the reactor operates with TOC reductions above 80% (or below 55%) decreasing the occurrence of chelating by-products such as dicarboxylic acids.

5. Acknowledgements

This research has been supported by CONICET (PIP-0575), UNMdP, ANPCyT (PICT1992-2014) (Argentina). The authors wish to thank Mr. Héctor Asencio and Mr. Pablo Kalafatovich for their technical assistance.

References

[1] B.L. Loeb, Water-Energy-Food Nexus, Ozone Sci. Eng. 38 (2016) 173–174. doi:10.1080/01919512.2016.1166029.

[2] R. Dewil, D. Mantzavinos, I. Poulios, M.A. Rodrigo, New perspectives for Advanced Oxidation Processes, J. Environ. Manage. 195 (2017) 93–99. doi:10.1016/j.jenvman.2017.04.010.

[3] M.A. Oturan, & J.J. Aaron, Advanced Oxidation Processes in Water/Wastewater Treatment: Principles and Applications. A Review, Crit. Rev. Environ. Sci. Technol. 44 (2014) 2577–2641. doi:10.1080/10643389.2013.829765.

[4] F. Duarte, V. Morais, F.J. Maldonado-Hódar, L.M. Madeira, Treatment of textile effluents by the heterogeneous Fenton process in a continuous packed-bed reactor using Fe/activated carbon as catalyst, Chem. Eng. J. 232 (2013) 34–41. doi:10.1016/j.cej.2013.07.061.

[5] F. Martínez, J.A. Melero, J.A. Botas, M.I. Pariente, R. Molina, Treatment of Phenolic Effluents by Catalytic Wet Hydrogen Peroxide Oxidation over Fe_2O_3/SBA-15 Extruded Catalyst in a Fixed-Bed Reactor, (2007) 4396–4405. doi: 10.1021/ie070165h.

[6] N. Al-Hayek, J.P. Eymery, M. Doré, CATALYTIC OXIDATION OF PHENOLS WITH HYDROGEN PEROXIDE, Water Res. 19 (1985) 657–666.

[7] P. Bautista, A.F. Mohedano, J.A. Casas, J.A. Zazo, J.J. Rodriguez, Highly stable Fe/γ-Al_2O_3 catalyst for catalytic wet peroxide oxidation, J. Chem. Technol. Biotechnol. 86 (2011) 497–504. doi:10.1002/jctb.2538.

[8] M. Muñoz, Z.M. de Pedro, N. Menendez, J.A. Casas, J.J. Rodriguez, A ferromagnetic γ-alumina-supported iron catalyst for CWPO. Application to chlorophenols, Appl. Catal. B Environ. 136–137 (2013) 218–224. doi:10.1016/j.apcatb.2013.02.002.

[9] S. Navalon, M. Alvaro, H. Garcia, Fenton catalysts based on clays, silicas and zeolites, Appl. Catal. B Environ. 99 (2010) 1–26. doi:10.1016/j.apcatb.2010.07.006.

[10] Y. Yan, S. Jiang, H. Zhang, Efficient catalytic wet peroxide oxidation of phenol over Fe-ZSM-5 catalyst in a fixed bed reactor, Sep. Purif. Technol. 133 (2014) 365–374. doi:10.1016/j.seppur.2014.07.014.

[11] A.N. Soon, B.H. Hameed, Heterogeneous catalytic treatment of synthetic dyes in aqueous media using Fenton and photo-assisted Fenton process, Desalination. 269 (2011) 1–16. doi:10.1016/j.desal.2010.11.002.

[12] C. di Luca, F. Ivorra, P. Massa, R. Fenoglio, Iron-alumina synergy in the heterogeneous Fenton-type peroxidation of phenol solutions, Chem. Eng. J. 268 (2015) 280–289. doi:10.1016/j.cej.2015.01.074.

[13] J. He, X. Yang, B. Men, D. Wang, Interfacial mechanisms of heterogeneous Fenton reactions catalyzed by iron-based materials: A review, J. Environ. Sci. 39 (2016) 97–109. doi:10.1016/j.jes.2015.12.003.

[14] H. Lim, J. Lee, S. Jin, J. Kim, T. Hyeon, Highly active heterogeneous Fenton catalyst using iron oxide nanoparticles immobilized in alumina coated mesoporous silica, 5 (2006) 463–465. doi:10.1039/b513517f.

[15] B. Kasprzyk-Hordern, Chemistry of alumina, reactions in aqueous solution and its application in water treatment, Adv. Colloid Interface Sci. 110 (2004) 19–48. doi:10.1016/j.cis.2004.02.002.

[16] B.N. Esteves, C.S.D. Rodrigues, L.M. Madeira, Wastewater Treatment by Heterogeneous Fenton-Like Processes in Continuous Reactors, in: Handb. Environ. Chem., Springer Berlin Heidelberg, Berlin, Heidelberg, 2017: pp. 1–45. doi:10.1007/698_2017_81.

[17] G. Eigenberger, W. Ruppel, Catalytic Fixed-Bed Reactors, Ullmann's Encycl. Ind. Chem. (2012). doi:10.1002/14356007.b04_199.pub2.

[18] J.A. Melero, F. Martínez, J.A. Botas, R. Molina, M.I. Pariente, Heterogeneous catalytic wet peroxide oxidation systems for the treatment of an industrial pharmaceutical wastewater., Water Res. 43 (2009) 4010–8. doi:10.1016/j.watres.2009.04.012.

[19] I. Mesquita, L.C. Matos, F. Duarte, F.J. Maldonado-hódar, A. Mendes, L.M. Madeira, Treatment of azo dye-containing wastewater by a Fenton-like process in a continuous packed-bed reactor filled with activated carbon, J. Hazard. Mater. 237–238 (2012) 30–37. doi:10.1016/j.jhazmat.2012.07.066.

[20] J.A. Botas, J.A. Melero, F. Martínez, M.I. Pariente, Assessment of Fe_2O_3/SiO_2 catalysts for the continuous treatment of phenol aqueous solutions in a fixed bed reactor, Catal. Today. 149 (2010) 334–340. doi:10.1016/j.cattod.2009.06.014.

[21] C. di Luca, P. Massa, R. Fenoglio, F.M. Cabello, Improved Fe_2O_3/Al_2O_3 as heterogeneous Fenton catalysts for the oxidation of phenol solutions in a continuous reactor, J. Chem. Technol. Biotechnol. 26 (2014) n/a-n/a. doi:10.1002/jctb.4412.

[22] F. Martínez, R. Molina, M.I. Pariente, J.A. Siles, J.A. Melero. Low-cost Fe/SiO_2 catalysts for continuous Fenton processes. Catal Today 280 (2017) 176–183]. doi: 10.1016/j.cattod.2016.04.044

[23] S. Perathoner, G. Centi, Wet hydrogen peroxide catalytic oxidation (WHPCO) of organic waste in agro-food and industrial streams, Top. Catal. 33 (2005) 207–224. doi:10.1007/s11244-005-2529-x.

[24] J.A. Melero, G. Calleja, F. Martínez, R. Molina, M.I. Pariente, Nanocomposite Fe_2O_3/SBA-15: An efficient and stable catalyst for the catalytic wet peroxidation of phenolic aqueous solutions, Chem. Eng. J. 131 (2007) 245–256. doi:10.1016/j.cej.2006.12.007.

[25] J. Levec, A. Pintar, Catalytic oxidation of aqueous solutions of organics. An effective method for removal of toxic pollutants from waste waters, Catal. Today. 24 (1995) 51–58.doi: 10.1016/0920-5861(95)00006-2.

[26] J.J. Delgado, J. a. Pérez-Omil, J.M. Rodríguez-Izquierdo, M. a. Cauqui, The role of the carbonaceous deposits in the Catalytic Wet Oxidation (CWO) of phenol, Catal. Commun. 7 (2006) 639–643. doi:10.1016/j.catcom.2006.02.003.

[27] J.A. Zazo, J.A. Casas, A.F. Mohedano, J.J. Rodríguez, Catalytic wet peroxide oxidation of phenol with a Fe/active carbon catalyst, Appl. Catal. B Environ. 65 (2006) 261–268. doi:10.1016/j.apcatb.2006.02.008.

[28] K. Fajerwerg, H. Debellefontaine, Wet oxidation of phenol by hydrogen peroxide using heterogeneous catalysis Fe-ZSM-5: A promising catalyst, Appl. Catal. B

Environ. 10 (1996) 229–235.doi:10.1016/S0926-3373(96)00041-0.

[29] X. Xue, K. Hanna, C. Despas, F. Wu, N. Deng, Effect of chelating agent on the oxidation rate of PCP in the magnetite/H_2O_2 system at neutral pH, J. Mol. Catal. A Chem. 311 (2009) 29–35.doi:10.1016/j.molcata.2009.06.016.

[30] G. Busca, S. Berardinelli, C. Resini, L. Arrighi, Technologies for the removal of phenol from fluid streams: A short review of recent developments, J. Hazard. Mater. 160 (2008) 265–288. doi:10.1016/j.jhazmat.2008.03.045.

[31] C. di Luca, P. Massa, R. Fenoglio, F.M. Cabello, Improved Fe2O3/Al2O3 as heterogeneous Fenton catalysts for the oxidation of phenol solutions in a continuous reactor, J. Chem. Technol. Biotechnol. 89 (2014) 1121–1128. doi:10.1002/jctb.4412.

[32] A.J. van Dillen, R.J.A.M. Terörde, D.J. Lensveld, J.W. Geus, K.P. de Jong, Synthesis of supported catalysts by impregnation and drying using aqueous chelated metal complexes, 216 (2003) 257–264. doi:10.1016/S0021-9517(02)00130-6.

[33] F. Mijangos, F. Varona, N. Villota, Changes in Solution Color During Phenol Oxidation by Fenton Reagent, 40 (2006) 5538–5543.doi:10.1021/es060866q.

[34] L.F. Liotta, M. Gruttadauria, G. Di Carlo, G. Perrini, V. Librando, Heterogeneous catalytic degradation of phenolic substrates : Catalysts activity, 162 (2009) 588–606. doi:10.1016/j.jhazmat.2008.05.115.

[35] M. Thommes, K. Kaneko, A. V. Neimark, J.P. Olivier, F. Rodriguez-Reinoso, J. Rouquerol, K.S.W. Sing, Physisorption of gases, with special reference to the evaluation of surface area and pore size distribution (IUPAC Technical Report), Pure Appl. Chem. 87 (2015) 1051–1069. doi:10.1515/pac-2014-1117.

[36] K. Lagarec, D.G. Rancourt, Mossbauer spectral analysis software, Version 1., Dep. of Phys-University of Ottawa, 1998.

[37] T. Preočanin, N. Kallay, Application of » Mass Titration « to Determination of Surface Charge of Metal Oxides, Croat. Chem. Acta. 71 (1998) 1117–1125.

[38] G. Larachi, B.P.. Grandjean, Excel worksheet simulator for flooded-bed reactor, Laval Univ. (n.d.). http://www.grandjean-bpa.com/pbrsimul/pbrsimul.html (accessed August 20, 2017).

[39] F.A.L. Dullien, Porous Media: Fluid Transport and Pore Structure, Second, ACADEMIC PRESS, INC., San Diego, California, 1991.

[40] L.S. Clesceri, A.E. Greenberg, A.D. Eaton, Standard Methods for the Examination of Water and Wastewater, 20th ed., American Public Health Association, 1998.

[41] Z. Zhang, R.W. Hicks, T.R. Pauly, T.J. Pinnavaia, Mesostructured Forms of γ-Al_2O_3, 124 (2002) 1592–1593.doi: 10.1021/ja016974o.

[42] R. Wischert, P. Laurent, C. Copéret, F. Delbecq, P. Sautet, γ-Alumina: The Essential and Unexpected Role of Water for the Structure, Stability, and Reactivity of "Defect" Sites, J. Am. Chem. Soc. 134 (2012) 14430–14449. doi:10.1021/ja3042383.

[43] G. Busca, The surface of transitional aluminas: A critical review, Catal. Today. 226 (2014) 2–13. doi:10.1016/j.cattod.2013.08.003.

[44] Y. Wu, F. Gao, B. Liu, Y. Dai, H. Zhu, B. Zhou, Y. Hu, L. Dong, Z. Hu, Influence of ferric oxide modification on the properties of copper oxide supported on γ-Al2O3, J. Colloid Interface Sci. 343 (2010) 522–528. doi:10.1016/j.jcis.2009.11.050.

[45] U. Schwertmann, R.M. Cornell. Iron Oxides in the Laboratory. Preparation and Characterization, Second, Completely Revised and Extended Edition, Wiley-VCH (2000).

[46] F. Bergaya, N. Hassoun, J. Barrault, L. Gatineau, PILLARING OF SYNTHETIC HECTORITE BY MIXED [AL13-xFEx] PILLARS, Clay Miner. 28 (1993) 109–122.doi:10.1180/claymin.1993.028.1.10.

[47] M.C. Biesinger, B.P. Paynec, A.P. Grosvenord, L.W.M. Laua, A.R. Gerson, R.St.C. Smart, Applied Surface Science 257 (2011) 2717–2730. doi: 10.1016/j.apsusc.2010.10.051

[48] T.S. Herng, W. Xiao, S.M. Poh, F. He, R. Sutarto, X. Zhu, R. Li, X. Yin, C. Diao, Y. Yang, X. Huang, X. Yu, Y.P. Feng, A. Rusydi, J. Ding, Nano Research, 8, 9 (2015) 2935-2945. doi:10.1007/s12274-015-0798-7.

[49] J. Mu, B. Chen, Z. Guo, M. Zhang, Z. Zhang, P. Zhang, Ch. Shao, Y. Liu, Nanoscale, 2011, 3, 5034. doi:10.1039/c1nr10972c.

[50] E. Murad, J.H. Johnston, Iron Oxides and Hydroxides, in: G.L. Long (Ed.), Mössbauer Spectrosc. Appl. to Inorg. Chem. Vol. 2, 1st ed., Plenum Publishing Corporation, 1987.

[51] R.E. Vandenberghe, E. De Grave, C. Landuydt, L.H. Bowen, Some aspects concerning the characterization of iron oxides and hydroxides in soils and clays, Hyperfine Interact. 53 (1990) 175–195. doi:10.1007/BF02101046.

[52] K. Jonás, K. Solymar, J. Zöldi, Some applications of Mössbauer spectroscopy for the quantitative analysis of minerals and mineral mixtures, J. Mol. Struct. 60 (1980) 449–452.doi:10.1016/0022-2860(80)80107-4.

[53] A. Paesano, C.K. Matsuda, J.B.M. da Cunha, M.A.Z. Vasconcellos, B. Hallouche, S.L. Silva, Synthesis and characterization of Fe-Al2O3 composites, J. Magn. Magn. Mater. 264 (2003) 264–274. doi:10.1016/S0304-8853(03)00215-4.

[54] L.A. Cano, M. V. Cagnoli, J.F. Bengoa, A.M. Alvarez, S.G. Marchetti, Effect of the activation atmosphere on the activity of Fe catalysts supported on SBA-15 in the Fischer-Tropsch Synthesis, J. Catal. 278 (2011) 310–320. doi:10.1016/j.jcat.2010.12.017.

[55] L.F. Cótica, S.C. Zanatta, S.N. de Medeiros, I.A. dos Santos, A. Paesano, J.B.M. da Cunha, Mechanical milling of the (α-Fe2O3) x(α-Al2O3)1-x system: an X-ray diffraction and Mössbauer spectral study, Solid State Ionics. 171 (2004) 283–288. doi:10.1016/j.ssi.2004.04.018.

[56] G.A. Waychunas, G.R. Rossman, Spectroscopic standard for tetrahedrally coordinated ferric iron: γ LiAlO2:Fe3+, Phys. Chem. Miner. 9 (1983) 212–215. doi:10.1007/BF00311957.

[57] J. Nawrocki, B. Kasprzyk-Hordern, The efficiency and mechanisms of catalytic ozonation, Appl. Catal. B Environ. 99 (2010) 27–42. doi:10.1016/j.apcatb.2010.06.033.

[58] A.L. Pham, C. Lee, F.M. Doyle, D.L. Sedlak, A Silica-Supported Iron Oxide Catalyst Capable of Activating Hydrogen Peroxide at Neutral pH Values, Environ. Sci. Technol. 43 (2009) 8930–8935.doi: 10.1021/es902296k.

[59] M. Kosmulski, The pH dependent surface charging and points of zero charge, J. Colloid Interface Sci. 253 (2002) 77–87. doi:10.1016/j.jcis.2014.02.036.

[60] B. Kasprzyk-Hordern, M. Ziółek, J. Nawrocki, Catalytic ozonation and methods of enhancing molecular ozone reactions in water treatment, Appl. Catal. B Environ. 46 (2003) 639–669. doi:10.1016/S0926-3373(03)00326-6.

[61] J. Carriazo, E. Guélou, J. Barrault, J.M. Tatibouët, R. Molina, S. Moreno, Catalytic wet peroxide oxidation of phenol by pillared clays containing Al-Ce-Fe, Water Res. 39 (2005) 3891–3899. doi:10.1016/j.watres.2005.06.034.

[62] L.C.A. Oliveira, M. Gonçalves, M.C. Guerreiro, T.C. Ramalho, J.D. Fabris, M.C. Pereira, K. Sapag, A new catalyst material based on niobia/iron oxide composite on the oxidation of organic contaminants in water via heterogeneous Fenton mechanisms, Appl. Catal. A Gen. 316 (2007) 117–124. doi:10.1016/j.apcata.2006.09.027.

[63] S.S. Lin, M. Gurol, Catalytic Decomposition of Hydrogen Peroxide on Iron Oxide : Kinetics , Mechanism , and Implications, Environ. Sci. Technol. 32 (1998) 1417–1423.doi:10.1021/es970648k.

[64] R. Chen, J.J. Pignatello, Role of quinone intermediates as electron shuttles in fenton and photoassisted fenton oxidations of aromatic compounds, Environ. Sci. Technol. 31 (1997) 2399–2406. doi:10.1021/es9610646.

[65] C. di Luca, Desarrollo de sistemas catalíticos para la oxidación de soluciones concentradas de contaminantes orgánicos con peróxido de hidrogeno., Universidad Nacional de Mar del Plata, 2015.

[66] D. Mantzavinos, E. Psillakis, Enhancement of biodegradability of industrial wastewaters by chemical oxidation pre-treatment, J. Chem. Technol. Biotechnol. 79 (2004) 431–454. doi:10.1002/jctb.1020.

[67] A.D. Bokare, W. Choi, Review of iron-free Fenton-like systems for activating H2O2 in advanced oxidation processes, J. Hazard. Mater. 275 (2014) 121–135. doi:10.1016/j.jhazmat.2014.04.054.

[68] G. Boczkaj, A. Fernandes, Wastewater treatment by means of advanced oxidation processes at basic pH conditions: A review, in: Chem. Eng. J. 320 (2017) 608–633. doi:10.1016/j.cej.2017.03.084.

[69] J.A. Zazo, G. Pliego, S. Blasco, J.A. Casas, J.J. Rodríguez, Intensification of the Fenton Process by Increasing the Temperature, Ind. Eng. Chem. Res. 2011,. 50 (2011) 866–870.doi:10.1021/ie101963k.

[70] W. Stumm, Chemistry of the solid-water interface, John Wiley & Sons, Inc., 1992.

[71] E. Baumgarter, M. Blesa, H. Marinovich, A. Maroto, Heterogeneous Electron Transfer as a Pathway in the Dissolution of Magnetite in Oxalic Acid Solutions, Norg. Chem. 22 (1983) 2224–2226.doi: 10.1021/ic00158a002.

[72] D. Panias, M. Taxiarchou, I. Paspaliaris, A. Kontopoulos, Mechanisms of dissolution of iron oxides in aqueous oxalic acid solutions, Hydrometallurgy. 42

(1996) 257–265.doi: 10.1016/0304-386X(95)00104-O.

[73] B. Gu, J. Schmitt, Z. Chen, L. Liang, J.F. McCarthy, Adsorption and desorption of different organic matter fractions on iron oxide, Geochim. Cosmochim. Acta1. 59 (1995) 219–229.doi: 10.1016/0016-7037(94)00282-Q.

[74] B.H. Gu, T.L. Mehlhorn, L.Y. Liang, J.F. McCarthy, Competitive adsorption, displacement, and transport of organic matter on iron oxide: II. Displacement and transport, Geochim. Cosmochim. Acta. 60 (1996) 2977–2992. doi:10.1016/0016-7037(96)00157-3.

[75] M.A. Ali, D.A. Dzombak, Effects of simple organic acids on sorption of Cu^{2+} and Ca^{2+} on goethite, Geochim. Cosmochim. Acta. 60 (1996) 291–304. doi: 10.1016/0016-7037(95)00385-1.

[76] P.C. Hidber, T.J. Graule, L.J. Gauckler, Influence of the dispersant structure on properties of electrostatically stabilized aqueous alumina suspensions, J. Eur. Ceram. Soc. 17 (1997) 239–249. doi:10.1016/S0955-2219(96)00151-3.

[77] Y.S. Hwang, J.J. Lenhart, Dicarboxylic acid transport through hematite-coated sand, Chemosphere. 78 (2010) 1049–1055. doi:10.1016/j.chemosphere.2009.11.028.

[78] S. Desset-Brèthes, B. Cabane, O. Spalla, Competition between ligands for Al_2O_3 in aqueous solution, J. Phys. Chem. A. 116 (2012) 6511–6518. doi:10.1021/jp212359q.

[79] W. Jianguo, Z. Jiayu, P. Li, The role of competitive adsorbate in the impregnation of platinum in pelleted alumina support, Stud. Surf. Sci. Catal. 16 (1983) 57–67. doi:10.1016/S0167-2991(09)60009-4.

[80] J.A. Bergwerff, A.A. Lysova, L. Espinosa-Alonso, I. V. Koptyug, B.M. Weckhuysen, Monitoring transport phenomena of paramagnetic metal-ion complexes inside catalyst bodies with magnetic resonance imaging, Chem. - A Eur. J. 14 (2008) 2363–2374. doi:10.1002/chem.200700990.

[81] P. Munnik, P.E. De Jongh, K.P. De Jong, Recent Developments in the Synthesis of Supported Catalysts, Chem. Rev. 115 (2015) 6687–6718. doi:10.1021/cr500486u.

Figures

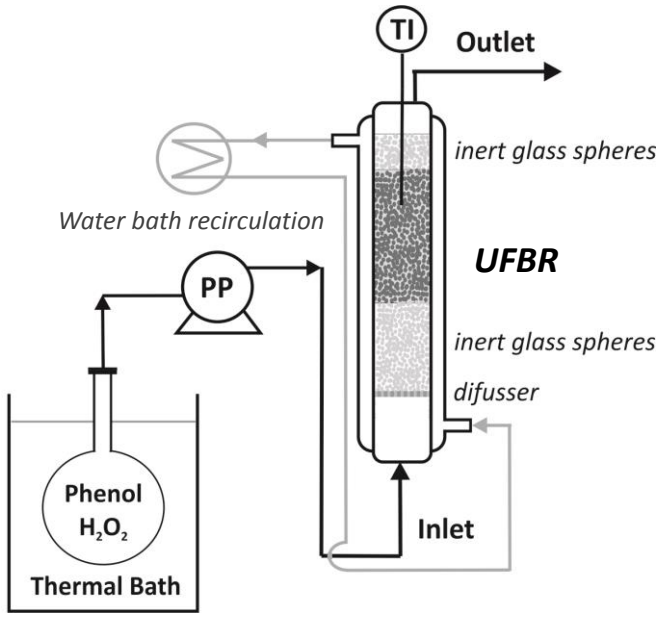

Figure 1. Experimental set-up employed for the CWHPO of phenol carried out under continuous operation (where TI: temperature indicator; PP: peristaltic pump).

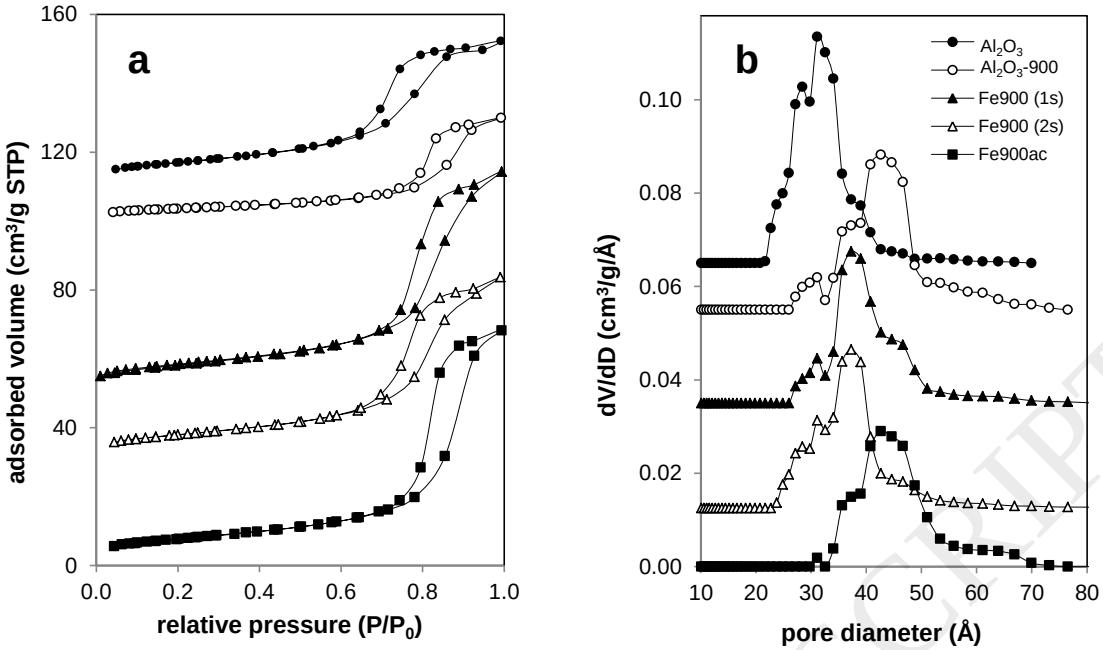

Figure 2. N_2 physisorption results: isotherms at -196 °C (a) and pore size distribution (b) for alumina support and fresh catalyst samples.

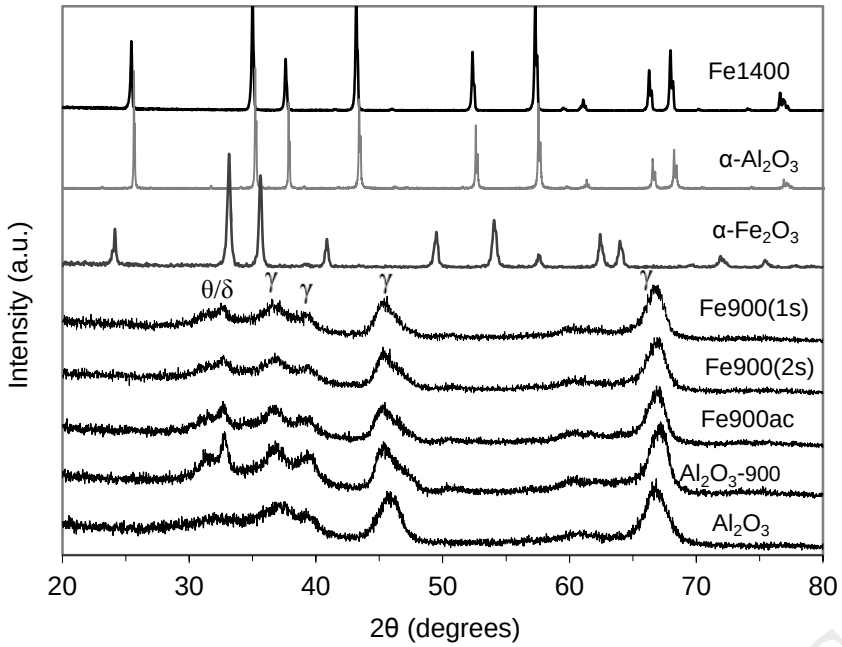

Figure 3. XRD diffractograms of the Fe-Al catalytic system calcined at 900 °C and 1400 °C. Corundum and hematite patterns were also include for comparative purposes. (Notation: θ/δ corresponds to θ-Al_2O_3 or δ-Al_2O_3 respectively; γ corresponds to γ-Al_2O_3).

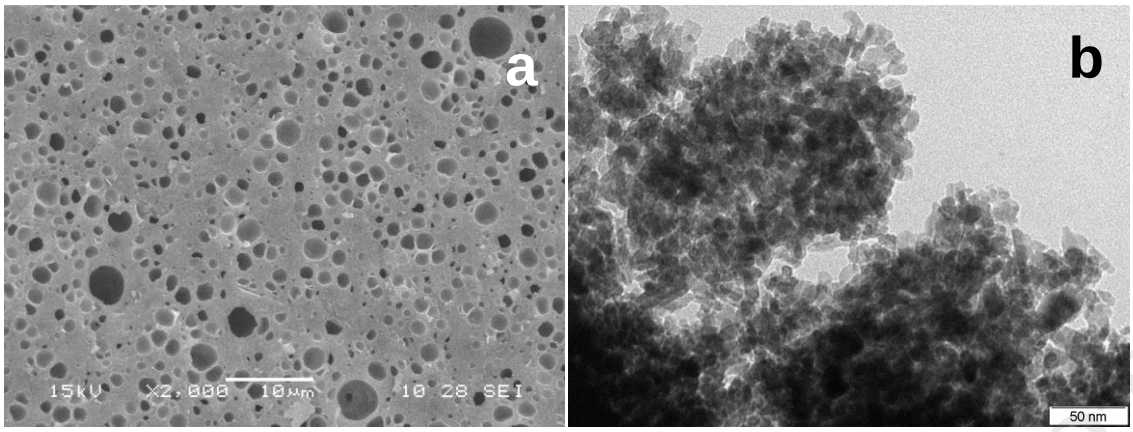

Figure 4. SEM (a) and TEM (b) images for Fe900ac catalyst.

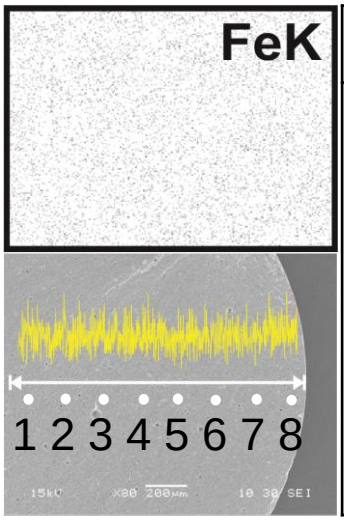

Pellet position	Fe content (wt %)
1	5.97
2	6.21
3	5.87
4	5.85
5	6.16
6	5.53
7	6.75
8	7.40
Outer shell	7.80

Figure 5. EDAX mapping, FeK profile across the spherical pellet and Fe content (wt%) from EDAX determinations at different pellet regions for Fe900ac catalyst (Internal zone: 1-8 and spherical cap).

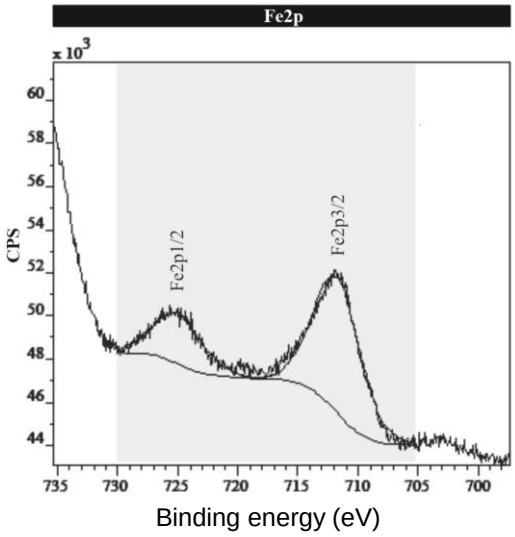

Figure 6. XPS results for Fe900ac catalyst, Fe2p core level deconvolution.

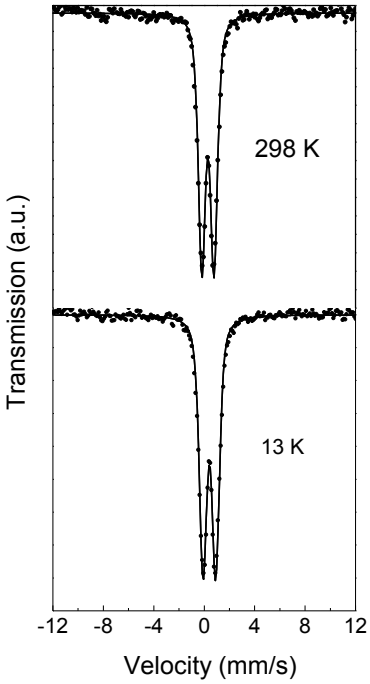

Figure 7. Mössbauer spectra of the Fe900ac catalyst at room temperature and 13 K.

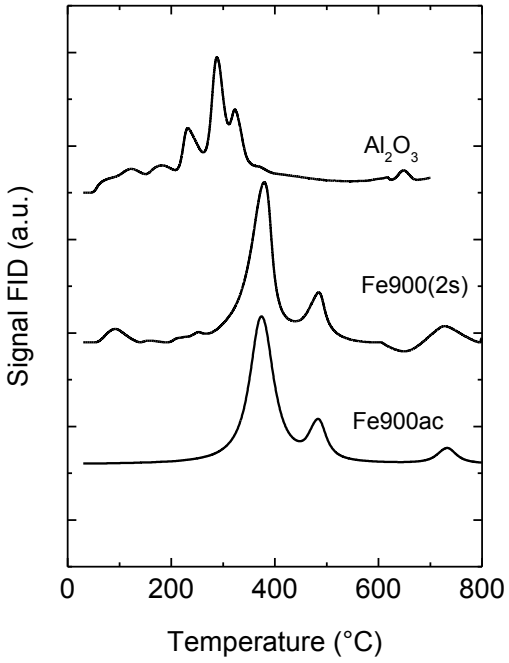

Figure 8. Temperature programmed desorption of pyridine of saturated samples.

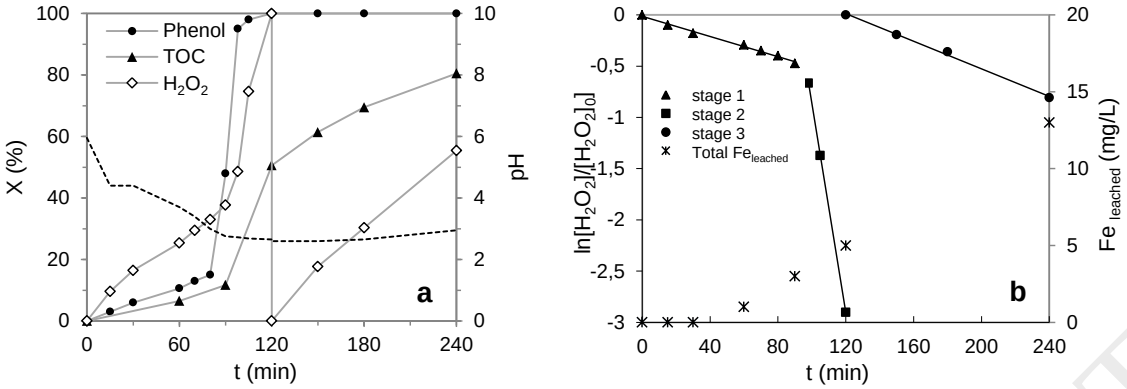

Figure 9. CWHPO of phenol in a batch reactor ([Catalyst] = 10 g/L, $[Phenol]_0$= 1 g/L, $[H_2O_2]$:[Phenol] = 14, pH_0 = 6 and T = 70 °C).

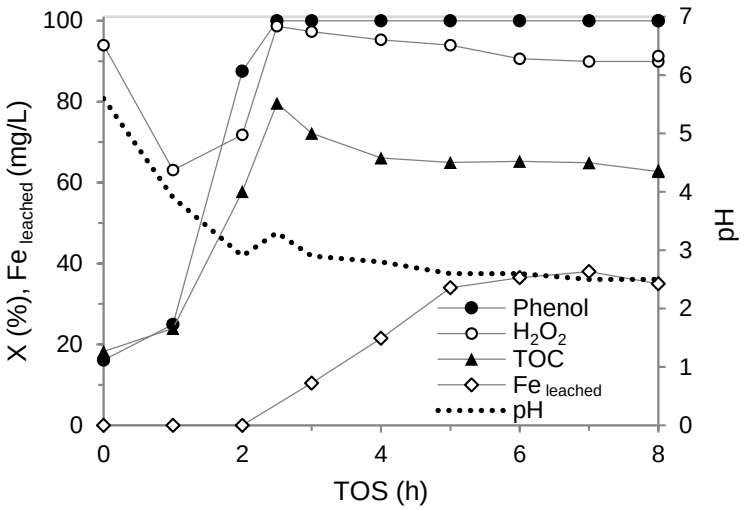

Figure 10. Conversion profiles of phenol peroxidation in a continuous UFBR reactor (T = 70 °C, W_{cat} = 20 g, Q_L = 5 mL/min, $[Phenol]_0$ = 1 g/L, $[H_2O_2]$:[Phenol] = 14 and pH_0 = 3).

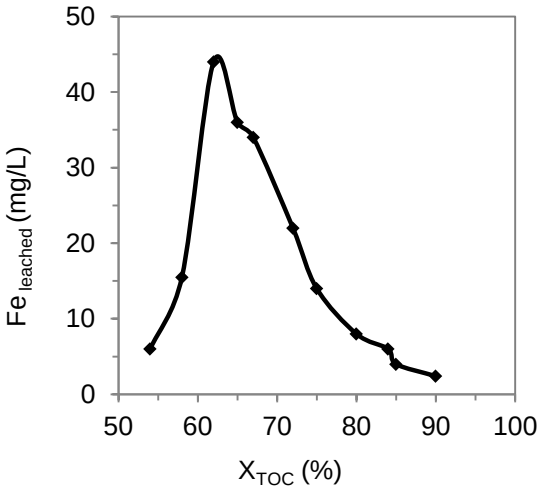

Figure 11. Fe concentration vs. TOC conversion in the outlet effluent for different operating conditions by using a continuous UFBR reactor (according to Table 5).

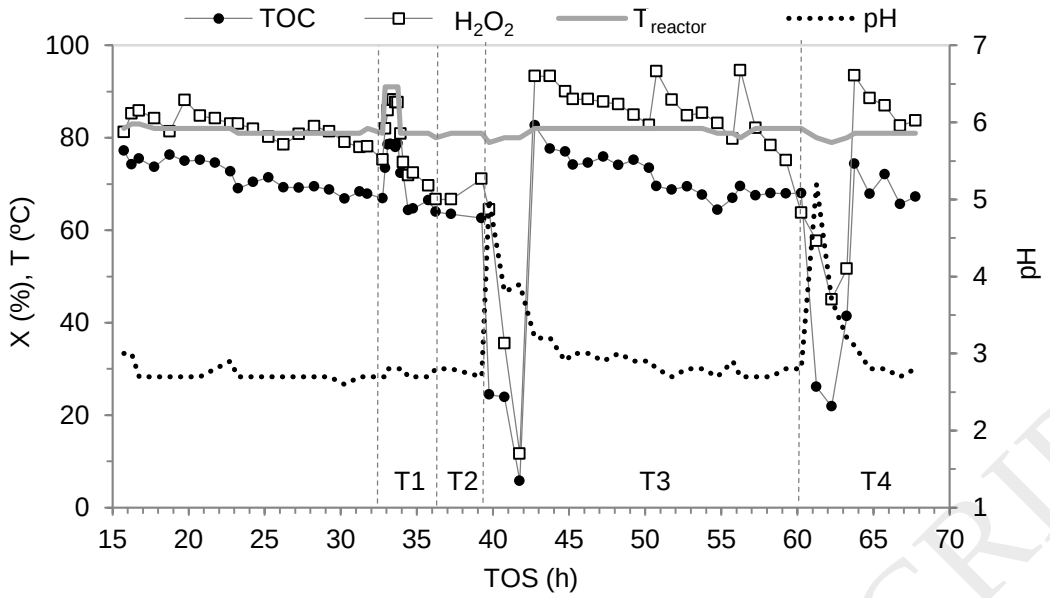

Figure 12. Long-term phenol peroxidation by using a continuous UFBR reactor (T = 80 °C, W_{cat} = 20 g, Q_L = 5 mL/min, $[Phenol]_0$ = 1 g/L, $[H_2O_2]$:[Phenol] = 16.8 and pH_0 = 6).

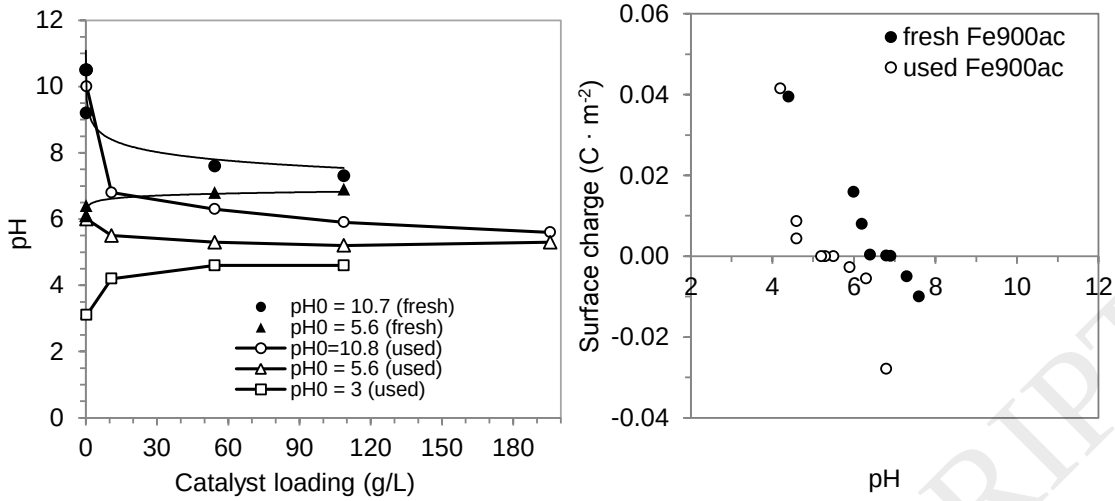

Figure 13. Mass titration at different initial pH of the water to which pelletized solid samples was added and surface charge density calculated from mass titration data for the fresh and used Fe900ac catalyst (c.a. 70 h of usage under continuous mode at the UFBR).

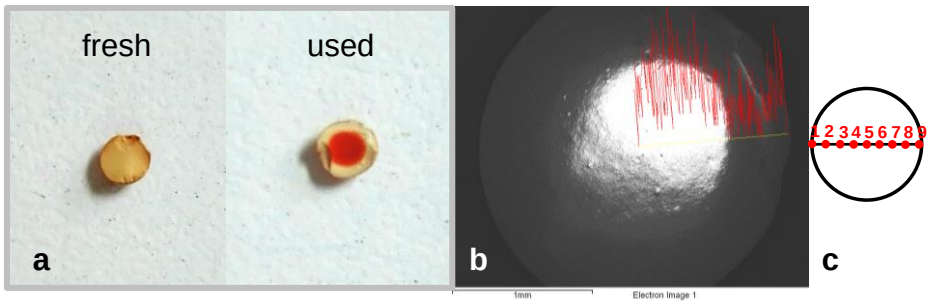

Position	Fe (wt%)
1 (edge)	5.1
2	2.1
3	3.9
4	2.9
5 (center)	2.9
6	4.9
7	4.2
8	2.4
9 (edge)	3.4

Figure 14. Images for Fe900ac pellets sectioned equatorially: a) Image of fresh and used catalyst calcined at 500 °C; b) EDAX FeK profile across an used catalyst pellet; c) Fe content (wt%) from EDAX determinations at different pellet regions.

Tables

Table 1. Operating conditions and reactor dimensions.

W_{cat}	6.7 − 20 g
Z	3.5 − 11 cm
T	60 − 90 °C
$[H_2O_2]$:[Phenol]	14 − 16.8 mol/mol
Q_L	1.2 − 5 mL/min
θ	1.1 – 15 min
D_p	2.5 mm
D_i	2.3 cm
L	21 cm

Table 2. Summary of Fe content and N_2-physisorption results.

Sample	**Description**	**$Fe_{content}$ (wt%)**	**A_{BET} (m^2/g)**	**V_{pore} (cm^3/g)**	**D_{pore} (Å)**
Al_2O_3	As received from SASOL	-	208	0.49	31
Al_2O_3-900	Al_2O_3 calcined at 900ºC	-	138	0.46	43
Fe900(1s)	Impregnated in 1 stage and calcined at 900ºC	6.6	125	0.38	37
Fe900(2s)	Impregnated in 2 stages and calcined at 900ºC	6.6	140	0.40	37
Fe900ac	Impregnated in 2 stages, calcined at 900ºC, acid washed and re-calcined at 900ºC	6.1	116	0.41	43

Table 3. Fe900ac hyperfine Mössbauer parameters obtained from spectra measured at 298 K y 13 K.

Temperature (K)	**δ (mm/s)**	**Δ (mm/s)**
298	0.29 ± 0.01	0.97 ± 0.01
13	0.41 ± 0.01	1.01 ± 0.01

δ: isomer shift (all isomer shifts are referred to α-Fe at 298 K); Δ: quadrupole splitting.

Table 4. Pseudo-first order apparent rate constant values for H_2O_2 decomposition with Fe900ac catalyst ([Catalyst] = 10 g/L, $[H_2O_2]_0$= 0.149 mol/L and pH_0 = 5).

T (°C)	**k_{ap} (min^{-1})**	**R^2**
60	0.0104	0.9981
70	0.0170	0.9995
80	0.0216	0.9985
90	0.0330	0.9966

Table 5. Summary of results for phenol peroxidation (1 g/L) at different operating conditions in a continuous UFBR reactor.

SS	T (ºC)	Q_L (mL/min)	θ (min)	R	pH_0	W_{cat} (g)	Z (cm)	X_{Phenol} (%)	X_{H2O2} (%)	X_{TOC} (%)	UV_{254}	pH_{out}	$Fe_{leached}$ (mg/L)	$Fe_{leached}$ (%)	η (%)	Expected lifetime (h)
1	60	5	3.7	14	6	20	11	98	58	54	-	2.6	6	0.1	93	678
2	60	2.5	7.3	14	6	20	11	99	70	58	-	2.7	15.5	0.3	83	525
3	70	5.4	1.1	14	6	6.7	3.5	98	70	44	-	2.9	-	-	63	-
4	70	5.4	2.3	14	6	13.3	7	100	93	60	-	2.6	-	-	65	-
5	70	5	3.7	14	6	20	11	100	100	62	0.55	2.7	44	2.0	62	92
6	70	5	3.7	14	3	20	11	100	92	65	0.52	2.6	36	3.3	71	113
7	70	5	3.7	16.8	6	20	11	100	88	67	0.51	2.7	34	4.5	63	120
8	70	2.5	7.3	16.8	6	20	11	100	95	72	0.31	3	22	4.8	63	370
9	80	5	3.7	16.8	6	20	11	100	92	75	0.24	2.8	14	5.3	68	290
10	80	2.5	7.3	16.8	6	20	11	100	97	80	0.13	3.2	8	5.4	69	1017
11	90	5	3.7	16.8	6	20	11	100	92	84	0.12	3.1	6	5.6	76	678
12	90	2.5	7.3	16.8	6	20	11	100	98	85	0.08	3.3	4	5.7	72	2033
13	90	1.2	15	16.8	6	20	11	100	99	90	0.04	3.5	2.4	5.7	76	7060

* Where abbreviations in first row means: SS: steady state reference point; T: temperature; Q_L: feed flow rate; θ: residence time; R: H_2O_2 to phenol molar ratio; pH_0: initial pH; W_{cat}: catalyst load; Z: bed height; X: conversion; UV_{254}: dimensionless aromaticity; pH_{out}: output pH; $Fe_{leached}$: leached iron expressed as output concentration or cumulated percentage of Fe loss and η: hydrogen peroxide consumption efficiency.